Ore Geology Reviews 101 (2018) 966–984

Contents lists available at ScienceDirect

Ore Geology Reviews

journal homepage: www.elsevier.com/locate/oregeorev

Part I: A resource estimation based on mineral system modelling prospectivity approaches and analogical analysis: A case study of the MVT Pb-Zn deposits in Huayuan district, China

Nan Li[a,b,*], Keyan Xiao[a,b], Li Sun[a,*], Shengmiao Li[d], Jianwei Zi[c], Kun Wang[a], Xianglong Song[a], Jianhua Ding[a], Cangbai Li[a]

[a] MLR, Laboratory of Metallogeny and Mineral Resource Assessment, Institute of Mineral Resources, Chinese Academy of Geological Sciences, Beijing 100037, China
[b] Centre for Exploration Targeting, ARC Centre of Excellence for Core to Crust Fluid Systems, The University of Western Australia, 35 Stirling Highway, Crawley, WA 6009, Australia
[c] Department of Applied Geology, Curtin University, Kent Street, Bentley, WA 6102, Australia
[d] Mineral Branch of Hunan Institute of Geological Survey, Changsha 410116, Hunan, China

ARTICLE INFO

Keywords:
Undiscovered resources assessment
Mineral system approach
Mineral deposit model
Modelling
Volumetric method

ABSTRACT

Several techniques have been proposed to predict undiscovered mineral resources at the regional scale by integrating multiple spatial datasets and mineral deposit models using Geographical Information Systems (GIS). An unresolved issue, however, is that predictive proxies are two-dimensional GIS layers at a regional scale, whereas mineralising processes occur in four dimensions (i.e., space and time). In the past 10 years, mineral system modelling approaches have been proposed and developed for the critical doubt that are described in terms of two characteristics: spatial scales and relevant geochemical processes. This paper demonstrates the modelling and combination of multiple scales based on mineral system prospectivity analysis and then present a resource estimation method that involves the calculation of three variables. In applying a GIS-based approach to a mineral system, we compared the resource estimation in a trap on the district scale to the extrapolation of reserve estimations of representative deposits in the same mineral system. The procedure used for the implementation of this method includes: (i) the incorporation of a descriptive model based on the mineral deposit type; (ii) the digitalization of the favourable characteristics of the type of investigated deposit; (iii) the implementation of the mineral system theory (approach) to pinpoint the locations of potential structural or stratigraphic traps at the district scale using GIS-based two-dimensional prospectivity mapping; (iv) the calculation of similarities and ore-bearing ratios; (v) the restructuring of models of favourable features at multiple scales (i.e., district and ore deposit scales); and (vi) the assessment of undiscovered mineral resources in traps. This method was used to estimate MVT-type Pb-Zn mineralisation in a promising potential region in northwestern Hunan Province, China. In addition, this study is divided into two parts, and this paper mainly describes the methodology.

1. Introduction

Geographic Information System (GIS)-based mineral potential mapping has become an active area of research, and a wide range of procedures have been developed (e.g., Bonham-Carter and Agterberg, 1989; Agterberg, 1993; Bonham-Carter, 1994; Singer and Kouda, 1996; Cheng et al., 1996; 2007; 2015; Knox-Robinson, 2000; Singer and Kouda, 2001; Cheng and Agterberg, 1999; Wang et al., 1990; Zhu, 1997; Brown et al., 2000; Zhao et al., 2001; Zhao, 2002; Zhao et al., 2003; Carranza et al., 2005, 2008, 2009; Porwal et al., 2003a,b,c; 2004; 2006a; 2006b; Singer and Menzie, 2010). Such approaches are now widely used to delineate mineral potential maps at regional scales. Based on the above procedures, the critical components of GIS-based mineral potential mapping have been summarized by Porwal and Carranza (2015) as: (i) the development of a conceptual geological and metallogenic model; (ii) the collection of data and construction of models (maps); and (iii) the integration of representative predictive models. In addition, high-quality mineral potential maps depend on available conceptual genetic models and how well predictive maps reflect mineralising processes.

Mineral system modelling approaches are useful for assessing the likelihood of mineral resources (Porwal et al., 2010; González-Álvarez

* Corresponding authors at: MLR, Laboratory of Metallogeny and Mineral Resource Assessment, Institute of Mineral Resources, Chinese Academy of Geological Sciences, Beijing 100037, China.
E-mail addresses: Nan.Li@uwa.edu.au, LiNan@cags.ac.cn (N. Li), sunli0727@163.com (L. Sun).

https://doi.org/10.1016/j.oregeorev.2018.02.014
Received 2 December 2017; Received in revised form 6 February 2018; Accepted 8 February 2018
Available online 10 February 2018
0169-1368/

et al., 2010; Joly et al., 2012, 2015; McCuaig and Hronsky, 2014), which can be described in terms of two characteristics: spatial scales and relevant geochemical processes. Possible spatial scales include the craton scale, regional scale, district scale, and ore deposit scale. The foundation of this approach is the theory of mineral systems. A mineral system was defined by Wyborn et al. (1994) as "…all the geological factors that control the generation and preservation of mineral deposits, and stresses the processes that are involved in mobilising ore components from a source, transporting and accumulating them in more concentrated form, and then preserving them throughout the subsequent history". McCuaig et al. (2010) summarized the framework of the mineral system in a four-step process by linking the conceptual components with the data actually available to support practical exploration targeting. The details include (i) the critical processes that must occur for a mineral deposit to form; (ii) the constituent processes in which the critical processes can proceed; (iii) the geological indicator elements necessary to show that mineralising processes have taken place; and (iv) the necessary presence of mappable features that can be used to detect the targeting elements directly or by proxy.

After delineating targets as the above, many researchers have focused on estimating undiscovered mineral resources. Singer (1993) proposed the United States Geological Survey (USGS) 3-part method based on the mineral deposit model, which involves the combination of: (1) delineating areas based on the types of deposits possible in a geological setting; (2) estimating the characteristics and amount of mineral resources using the grade and tonnage model; and (3) estimating the number of each type of undiscovered deposit. This approach has been applied to different kinds of deposits and implemented in many countries to estimate the undiscovered mineral resources remaining in the ground. Other widely quantitative resource assessments used include the volumetric method (Kingston et al., 1978; Meyer, 1978; Drew, 1997; Boyer and Bai, 1998) and Zipf's Law (Merriam et al., 2004; Guj et al., 2011). In addition, some mathematical models can be used in assessments, such as deposit density models (Bliss and Menzie, 1993) and economic models (Singer, 1993). Of these, the volumetric methods defined by Kingston et al. (1978) and Meyer (1978) have been used to estimate undiscovered hydrocarbon resources in Indonesia and tin deposits in Britain.

In this paper, we demonstrate the value of mineral system modelling prospectivity analysis and then propose a resource estimation analogy method for undiscovered mineral resources based on the extrapolation of representative deposits. The primary process consists of recognizing ore-bearing zones and the association of favourable features at typical deposits (Fig. 1), analysing the mineral systems related to representative deposits, modelling their features, and estimating their resources. In this study, first, a trap was delineated by applying the GIS-based mineral system modelling approach from a regional scale to a district scale; second, undiscovered resources were estimated in the trap using Equation (7), which includes (i) calculating the ore-bearing ratio based on representative deposits; (ii) discussing the Similarity Index; and (iii) inferring the volume of the trap. In this paper, we focused on experimental mineral potential mapping for MVT-type Pb-Zn deposits in Huayuan district, Hunan Province, China.

In addition, the method documented in this contribution was tested and refined in several mineralised areas during the Chinese initiative known as the "The China National Mineral Resource Assessment" (Xiao et al., in press; Cong et al., in press; Cui et al., in press; Zhang et al., in press; Wang et al., 2017), which was funded by the China Geological Survey. The aim of the initiative was to estimate the resources of 25 major minerals in 25 significantly mineralised belts or zones, and it involved 30 Chinese organizations working in union (China Geological Survey, 2013).

2. Framework of resource estimation

2.1. Superiority methods

The resource estimation documented refers to two methods. One is the 3-part method proposed by Singer (1993), in which (i) the Grade-Tonnage model assesses the frequency distributions of ore tonnages and the average grades of well-explored deposits, respectively; (ii) permissive boundaries are delineated based on the mineral resource map; and (iii) the mineral deposit densities (Singer, 2008) in geologically similar settings are assessed. Essentially, in the above method, the estimates are internally consistent because the observed characteristics of the deposits are consistent with those in the descriptive models and grade and tonnage models. In the second part of the assessment, mineral deposit models (Cox and Singer, 1986) are used to classify mineralised and barren environments and to classify types of known deposits, whereas mineral deposits are distinguished from mineral occurrences during the estimation of the number of deposits. A wide variety of geoscience information from the region of interest is used for these tasks.

The second method is a volumetric method that is used to assess mineral resources that are subhorizontal to horizontal and have a uniform thickness (Fig. 2), such as those in hydrocarbon and sediment-hosted ore deposits (Kingston et al., 1978; Meyer, 1978). This method includes two critical steps to determine the mean volume of the host formation based on available geological evidence from past production, as well as the determination of whether or not the region being assessed has the same characteristics as those of the representative deposits. The method is based on the following assumptions: (i) the regions present are either explored or unexplored basins; (ii) the mean concentration of

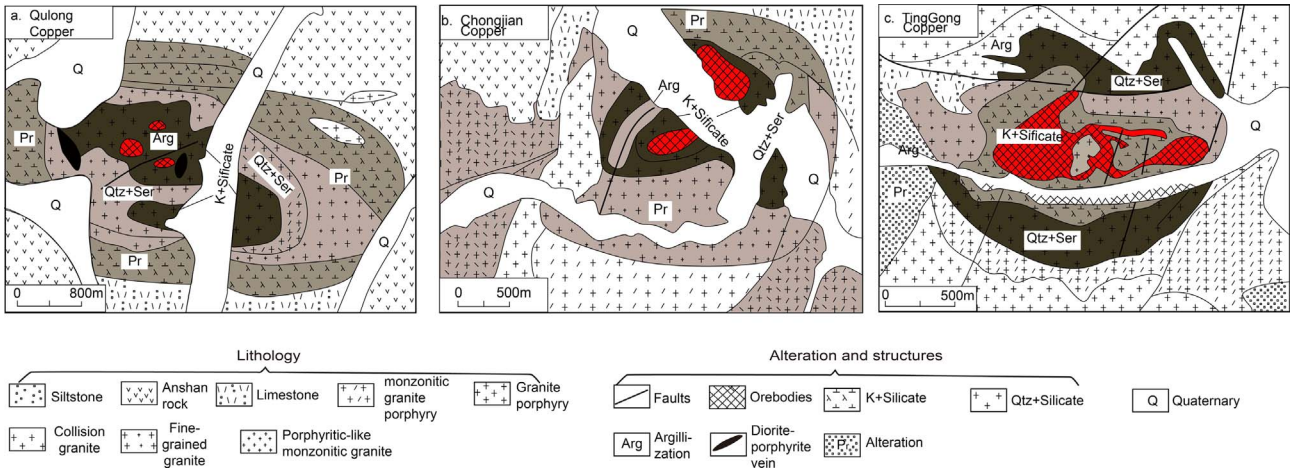

Fig. 1. Ore-bearing zones at the representative porphyry copper deposits.

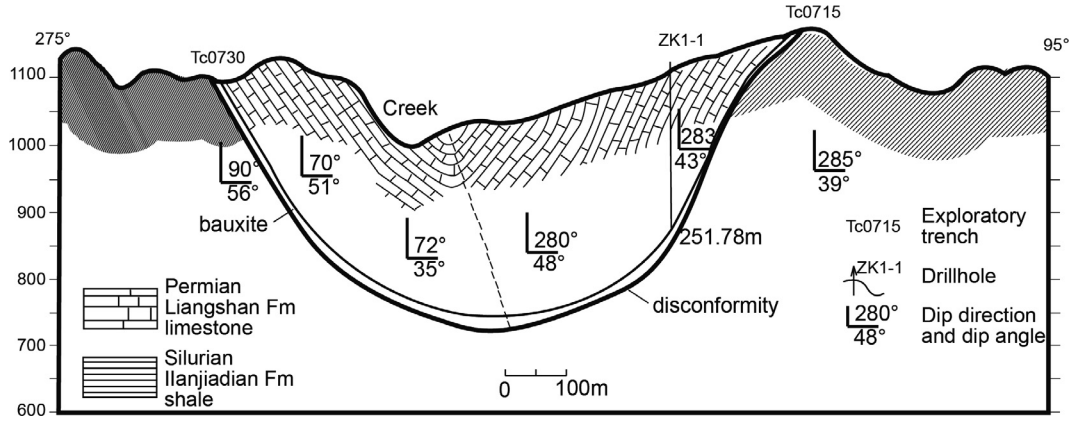

Fig. 2. Typical cross-section of a sedimentary deposit of bauxite (modified after Liu et al., 2010).

resources per unit or formation contains the average density (mass/volume) of the units in an explored basin; (iii) the mean density of the units or formations in an explored basin is equal to that in an unexplored basin; and (iv) unexplored basins are interpreted as traps with future petroleum potential.

The following equation defined by Kingston et al. (1978) is used to estimate the mineral resources in a prospective area:

$$W_{estimatedresources} = C \times V_{predictionvolume} \quad (1)$$

where C is the mean concentration, which is the ratio between the production and volume of a deposit, as shown in Eq. (2); $W_{estimated\ resources}$ is the total resource in the prediction area; and $V_{prediction\ volume}$ is the volume of the ore-forming geological body in the prediction area. The value of $V_{prediction\ volume}$ is equal to $S \times H$, where S is the project area of the ore and H is its thickness.

The formula for calculating the mean concentration (C) is:

$$C = \frac{rf\,(pp + pr + ir + ifr)}{vf - vx} \quad (2)$$

where rf is the recovery factor, pp is the past production, pr is the measured reserve, ifr is the inferred reserve, ir is the total resource, vx is the volume of the explored basin based on drilling, and vf is the volume of favourable rocks present at the deposit (Kingston et al., 1978).

2.2. Resource estimation analogy method

In this paper, we propose a resource estimation method based on mineral system modelling prospectivity analysis. One of the major characteristics of the mineral system approach is multiple spatial scales, including the craton, regional, district, and ore deposit scales. In this process, geologists first model favourable features and then delineate favourable areas from the craton scale to the district scale in an orderly fashion. Commonly, favourable areas are bounded by major structures, formations, and large rocks. For example, the Mississippi Valley-Type (MVT) Pb-Zn deposit represents a strata-bound deposit, and its favourable host rocks are carbonate formations. Additionally, on the ore deposit scale, geologists have constructed digital mineral deposit models, including those of its ore-bearing zones and orebodies. Ore-bearing zones always comprise rocks, alterations, and small structures. For instance, a porphyry copper is concealed by granite porphyry and contains evidence of alteration, such as diorite-porphyrite veins and K-silicates, which were defined as the ore-bearing zones of porphyry copper deposits (Fig. 1). Another example is that the MVT Pb-Zn deposit was concealed by limestone defined as an ore-bearing zone in the deposit. In summary, an assumption presented is that the mean resources per unit (e.g., m^3) in a favourable area (defined as a trap in the mineral system) are consistent with the known ore-bearing zones (defined as fluid sinks in the mineral system) in the same mineral system, in which ore-bearing zones and favourable areas have similar associations in terms of their geological features and ages. Following this assumption, the undiscovered mineral resources were estimated based on an analogy between the resources in favourable areas and those estimated in ore-bearing zones. On the other hand, however, the consistency of distribution is subtly different on a larger scale, i.e., a regional- or district-scale, compared to an ore deposit scale. It can be understood that the favourable area comprises cells with different levels of similarity.

The classic equation for reserve estimation in ore deposits contains three variables, namely, grade, proportion (or density), and volume. Compared to the above equation, as well as the analogy, the terminology used in this method includes: (i) the representative deposit is defined as a representative or well-explored deposit in a trap, as shown in Fig. 3. It is slightly different than the definition of a typical deposit in previous studies (Singer and Kouda, 1996; Singer, 2006); (ii) the terminologies of trap, fluid reservoir, favourable area, and permissive boundary describe the same object using different methodologies; (iii) the ore-bearing ratio represents the mean resources per unit from representative deposits; and (iv) the Similarity Index (or coefficient) is a quantification of how similar the association of favourable features in a trap is with the association of favourable features in representative ore deposits in the same mineral system. Using these definitions, the general equation for estimating the undiscovered resources assessment is presented in Eq. (3), where the mean ore-bearing ratio of multiple traps (R_{unit}) is multiplied by the volume of the traps (V_{trap}):

$$R_{trap} = R_{unit} \times V_{trap} \quad (3)$$

The mean ore-bearing ratio is determined using the following equation:

$$R_{unit} = \overline{G}_{grade} \times \overline{P}_{porportion} \cong \frac{\sum_i C_i \times S_i}{i} \quad (4)$$

where the ore-bearing ratio in the trap, R_{unit}, is theoretically calculated by multiplying the grade and proportion; however, obviously, it is hard to determine the grades and proportions in traps. These data are extrapolated from known ore deposits in the permissive boundaries by calculating their mean ore-bearing ratio. The ore-bearing ratio at a mineral deposit, C_i, is calculated as the measured resources divided by the volume of the ore-bearing zone and then multiplied by the similarity coefficient (S_i), with 'i' being the amount of representative deposits in the trap.

The ore-bearing ratio at a representative ore deposit is defined as:

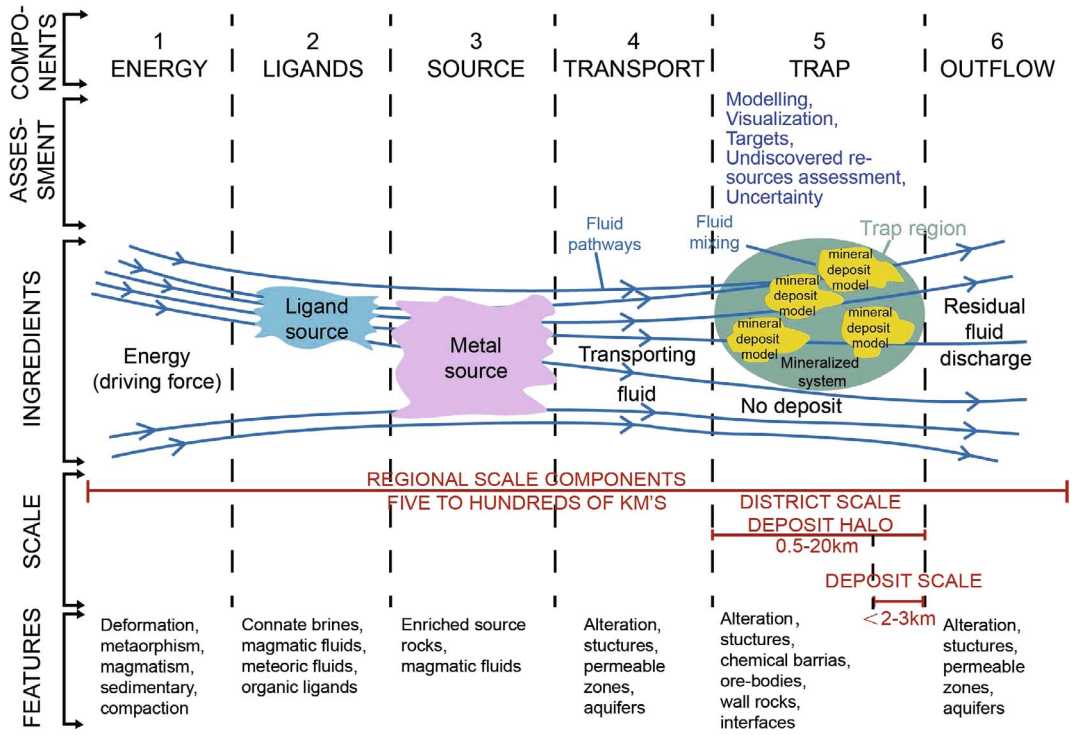

Fig. 3. Mineral system approach to delineate targets (modified after Hagemann et al. 2016).

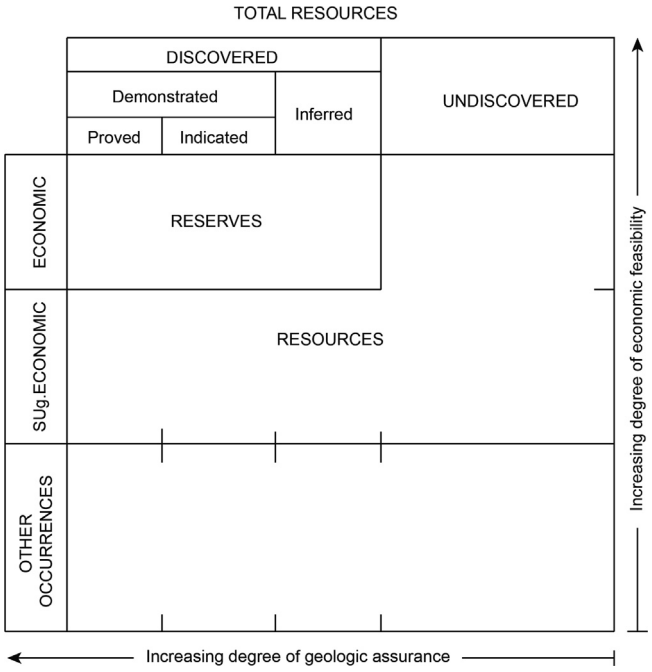

Fig. 4. Classification of resources (modified after Kingston et al., 1978).

$$C_i = \frac{R_{i.discovered}}{V_{i.depositmodel}} \tag{5}$$

where $R_{i.discovered}$ is the discovered resources at one of the representative deposits (Fig. 4), and $V_{depositmodel}$ is the volume of the mineralised zone. The size of a mineral deposit model includes both the orebodies and host rocks.

The volume of a trap is a function of the 3D permissive boundaries (Fig. 3), associated alteration, structural controls, chemical constraints, and nature of the wall rocks at the district scale. The undiscovered mineral resource in a trap (R_{trap}) is defined using the equations:

$$\begin{aligned} R_{trap} &= \frac{\sum_i C_i \times S_i}{i} \times V_{trap} \\ &= \frac{\sum_i \frac{R_{i.discovered}}{V_{i.depositmodel}} \times S_i}{i} \times V_{trap} \\ &= \frac{\sum_i \frac{R_{i.discovered}}{V_{i.depositmodel}} \times V_{trap} \times S_i}{i} \end{aligned} \tag{6}$$

In Eq. (6), $V_{depositmodel}$ and V_{trap} are the volumes of the representative mineral deposits and the trap, respectively, and S_i is the similarity between the properties of representative deposits and the trap containing the deposits (Fig. 3). The volume variables, $V_{depositmodel}$ and V_{trap}, can be calculated using either empirical values or measurements, as long as enough data can be collected at the ground surface and underground.

In this paper, the discrimination of the distribution of resources per unit within the same mineral system is quantitatively presented by comparing the similarities between theoretical mineral deposit models, representative deposits, and the association of favourable features in the trap in the study area. The similarity indexes obtained from the study area are used to mark the differences in R_{unit} at representative deposits and traps from a mineral system (i.e., $\frac{S_2}{S_1}$, where S_1 is the mean Similarity Index between descriptive mineral deposit models defined by Cox and Singer (1986)) and the favourable association at a typical deposit, and S_2 is an average of the Similarity Index between a mineral deposit model and a favourable association at the trap. Using these factors, the equation used for the assessment of undiscovered resources is modified as:

$$R_{trap} = \frac{\sum_i \frac{R_{i.discovered}}{V_{i.depositmodel}} \times V_{trap} \times \frac{S_{trap}}{S_i}}{i} \tag{7}$$

The above data indicate that the mineral deposit model, mineral systems, and volumes are the three major components of the analogical undiscovered mineral resources method presented (Fig. 5). Therefore, the variables needed include the ore-bearing ratio, similarity coefficient, and volumes of host rocks or ore-bearing formations at a deposit scale, as well as the volumes of traps in a district area.

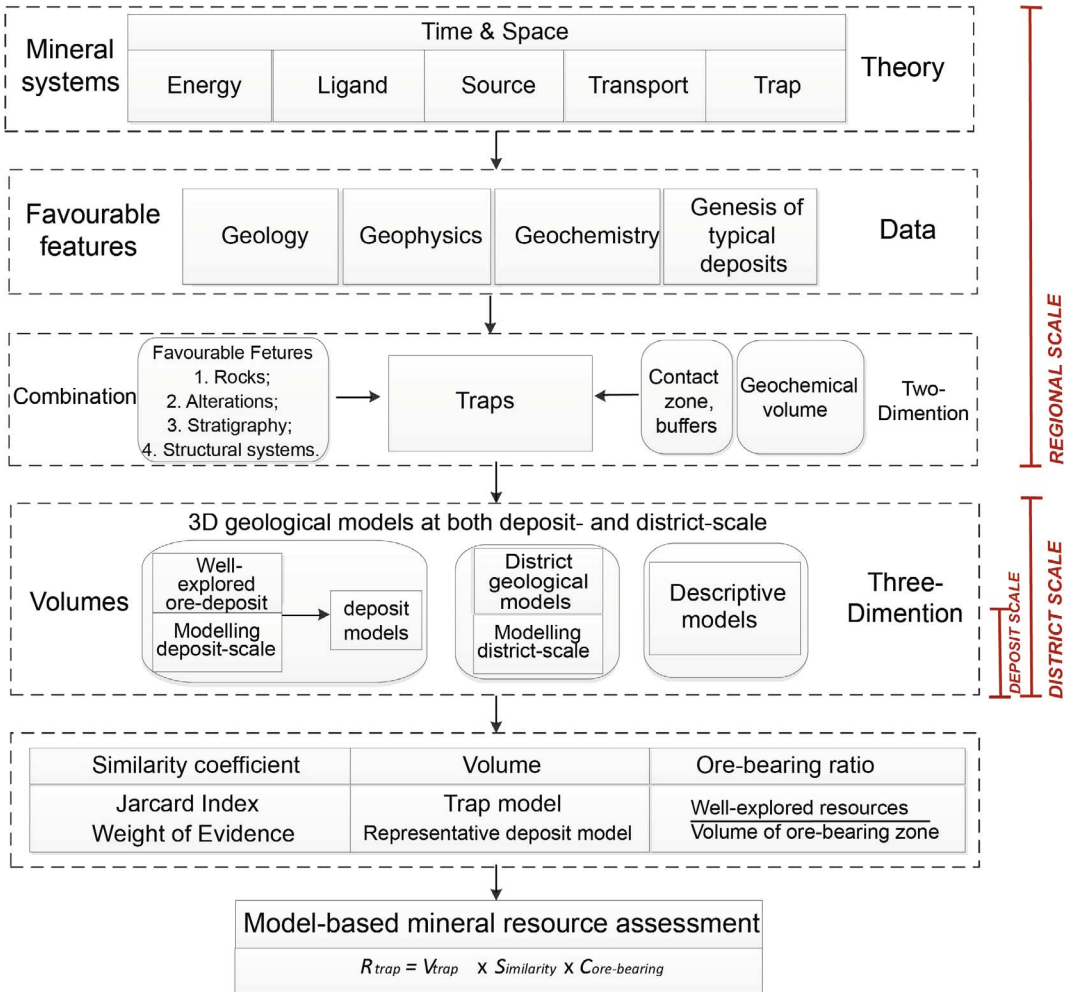

Fig. 5. Flow chart of the model-based improved volumetric method.

2.3. Volumetric calculation of ore-bearing zones and traps

2.3.1. Delineation of trap and volume calculations

Mineral systems comprise multiple scales and relevant chemical processes (Fig. 3). A trap can be regarded as a chemical scrubber or physical throttle (Joly et al., 2015). For example, volcanic associated massive sulfide deposits or skarn and carbonate replacement deposits are referred to as host rocks or traps where mineralisation accumulates within confined volumes. Joly et al. (2015) applied GIS-based 2D prospectivity modelling in Western Australia using conceptual mineral system models and emphasized the importance of realizing that these assessments do not necessarily point to the locations of concealed economic deposits. They are, however, intended as tools for developing exploration strategies by illustrating spatial variations in the geological characteristics of each type of deposit. This is done within the constraints or limitations of assumptions about the local geology and the ways in which such deposits form. Regional-scale datasets are critical for mapping the mineralising processes involved in the formation of mineral traps. As a result, while sources and pathways are typically well-represented in region-wide prospectivity modelling studies, traps are often less clearly resolved but can be better defined with GIS-based prospectivity mapping (Joly et al., 2015).

Based on the abovementioned studies, first, we used the same method presented in a study (Joly et al., 2015) that delineated targets based on GIS-based prospectivity mapping using 1:200,000-scale regional datasets. Second, on the district scale, geologists should refine the traps delineated at the regional scale based on higher-resolution and new multiple spatial-scale datasets because estimating traps is only one question at this scale (Joly et al., 2015).

There are two methods used to calculate the volume of a trap. The first is an empirical method in which the trap is seen as a regular geometric model. Thus, the volume of the trap can be calculated as the area (S) of the polygons of the trap on the ground multiplied by the estimated depth (H) of the trap determined from drillholes or geophysical data, as in Eq. (8).

$$V_{ideal} = s_{area} \times h_{depth} \tag{8}$$

Trap volumes can also be calculated by delineating their permissive boundaries, followed by the construction of 3D models to determine their volumes, which depends on the geometric characteristics of the deposit. The model-based method requires calculating two volumes using a 3D geometric model with the following equation:

$$V_{reality} = \frac{1}{3} \times \sum_{facei} \vec{x_i} \cdot \vec{n_i} \cdot t_i \tag{9}$$

where $\vec{x_i}$ is the jth-faced centroid, $\vec{n_i}$ is its normal vector forward to the outside, and t_i is the area of the face, which is currently a triangle in this equation. The method used to calculate volume using 3D modelling technology will be discussed in the part II.

2.3.2. Volume of representative deposits

In a mine, inferring the volume of an ore-bearing zone (Fig. 1) is not difficult because there is a sufficient number of drillholes, infrared spectrum collections, and even higher-resolution geophysical datasets.

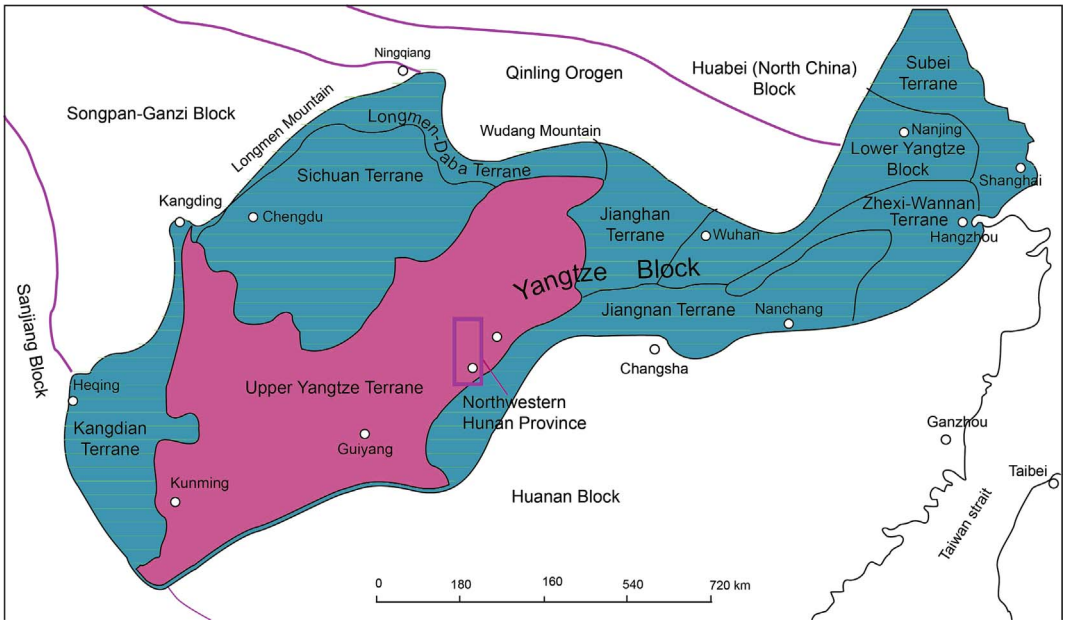

Fig. 6. Geotectonic classification in the Yangtze continental block.

As seen in Eqs. (8) and (9), there are two ways to calculate volumes $V_{i,depositmodel}$. In the first, the zone is seen as a regular geometric model and the depth is estimated using drillhole data; in the second, 3D models of the ore-bearing zone are created and then used to calculate volume.

2.4. Similarity Index

According to the mineral deposit model, ideally, deposit models provide necessary and sufficient information with which to discriminate possible mineralised environments from barren environments, types of known ore-bearing zones from each other, and mineral deposits from mineral occurrences. There are similar geological environments, rock types, age ranges, tectonic settings, associated deposit types, alterations, and geochemical signatures between favourable areas and representative ore-bearing zones from the same mineral system. Thus, subtle differences between favourable features in favourable areas and representative mineral deposits are defined using the Similarity Index or coefficient, which assumes that the mean resources per unit (e.g., m^3) in an ore-forming favourable zone are consistent with ore-bearing zones in known ore deposits (or fluid sinks in a mineral system) in the same mineral system. Several methods can be employed to calculate similarity coefficients, such as the Jaccard Index or weights of evidence, which are described as follows.

The Jaccard Index is known as Intersection over Union or the Jaccard similarity coefficient (Jaccard, 1901). This index is a statistic used to compare the similarity and diversity of sample sets, and it measures the similarity between finite sample sets. This is defined as the size of the intersection divided by the size, as expressed in the following equation, where A and B are sets:

$$J(A,B) = \frac{|A \cap B|}{|A \cup B|} = \frac{|A \cap B|}{|A| + |B| - |A \cup B|} \quad (10)$$

Weights of evidence (WofE) is commonly used when favourable characteristics are present at a typical deposit, which are the same as those in theoretical mineral deposit models (Cox and Singer, 1986). Prior to 2015, WofE was limited by Bayes' Rule, which describes the probability of an event based on prior knowledge of the conditions that might be related to the event. Cheng (2015) introduced the variant "BoostWofE", which integrates the Adaboost algorithm and typical WofEs so that the conditional independency test can be avoided. The equation for BoostWofE is:

$$O(D = 1|B_1 B_2 \ldots B_N) = O(D) \frac{P(B_1|D = 1)}{P(B_1|D = 0)} \prod_{k=2}^{N} \frac{P(B_k|B_1 \ldots B_{k-1} D = 1)}{P(B_k|B_1 \ldots B_{k-1} D = 0)} \quad (11)$$

The S_{trap} value in Eq. (7) can be calculated based on the composition of favourable features inside traps and the descriptive model (Cox and Singer, 1986). The S_i value can be obtained based on the favourable characteristics of a typical deposit, *i*, and the descriptive model. Furthermore, the $\frac{S_{trap}}{S_i}$ ratio can be calculated, as can WofE, if the S_i value is equal to 1.

2.5. Ore-bearing ratio

As outlined in Section 2.2 and expressed by Equations (4) and (5), the ore-bearing ratio is related to three variables i.e., $R_{i\_discovered}$, $V_{i\_depositmodel}$, and S_i. $R_{i\_discovered}$ denotes the resource in a representative mineral deposit within a mineral system; $V_{i,depositmodel}$ is the volume of a representative mineral deposit within a mineral system; and S_i is the association of favourable features from a mineral deposit model (Cox and Singer, 1986) or exploration. In this paper, the ore-bearing ratio is equal to the arithmetic mean based on representative deposits.

3. Study district

An example is presented below using 3D-modelling techniques and the improved volumetric method to estimate the undiscovered resources of stratabound deposits in the Huayuan district, covering an area of ~432 km^2 in Hunan Province, China.

3.1. Geological setting

The Huayuan district contains a significant concentration of Pb-Zn mineralisation. This area is located in the Bamianshan Orogen (fold belt), which is related to the Ordovician to Devonian convergence of the southeastern margin of the Yangtze Block, and the western part of the Jiangnan Terrane (Fig. 6).

The Huayuan area has a long geological history and contains sedimentary units located in the northwestern part of an arc-shaped structure in northwestern Hunan Province. The geological units in the

Table 1
Comparative table between typical MVT Pb-Zn and Pb-Zn deposits in NW Hunan Province, China (modified after Zhong and Mao, 2007b).

Features	Typical MVT Pb-Zn ore deposit	Pb-Zn ore deposits at north-west Hunan province, China
Regional tectonic setting	In the carbonate platform along the basin margin, and partially in the rift	Enriched in Paleozoic large sedimentary basin along the south east margin of Yangze Platform
Host stratigraphy Lithology	Mainly in the Paleozoic, Triassic thick sedimentary rock formation (e.g. dolomite and biogenic reef carbonate), others in the Proterozoic	Mainly hosted in Cambrian and Ordovician carbonate with thickness of ~5000 m, i.e. widely developed dolomite and other shallow water carbonate facies together with biogenic reef facies n the platform cover folds and closely related to Yanshanian tectonic activities with smooth strata formation
Relation between tectonic activities and ore deposit	Ore forming process in close relation with orogenic activities or tectonic collision with weak rock deformation and metamorphism for the ore deposits	
Deposit Distribution	Widespread mineralization forming large ore belts	Range of mineralization belts about tens of thousands square kilometres
Ore body morphology	Layer bound characteristic of the mineral ore controlled by stratum, stratoid and lenticular morphology	Main ore body controlled by stratum and stratoid morphology in consistent with wall rock occurrence both dominated by the interlayer fracture
Host structures	Various open gaps includingstructural fissures, unconformity surface and so on	Interlayer fracture, structural fissures, and faults
Mineral assemblage	Simple mineral assemblage of sphalerite and galena, and minor amounts of disseminated pyrite and chalcopyrite	Simple composition such as sphalerite and galena with other minor minerals
Wall rock alteration	Carbonate-, dolomite-, silica-, Fe- and fluorite-alteration	Mainly controlled by carbonate-, dolomite- and silica-alteration
Ore grade	Pb + Zn: ~5–15% Zn as the main element accompanied by Ag and Cu	Pb + Zn: ~3–10% Zn as the main element accompanied by Ag、Cd and Cu.
Ore structure	Fine- to coarse-grained, massive, brecciated, disseminated and veins with metasomatic and dissolution textures	Various grain and metasomatic structure with metasomatic, patch and disseminated texture
Ore deposit scale	Mainly small- and medium-size deposits distribute in groups with some large ore deposits	Appraised 1 large deposit and 5 small and medium size deposits with promising prospectivity
Pb, Sisotope	$\delta^{34}S$: ~ +10 ± 25‰; enriched heavy S is derived from marine evaporates with no distinct characteristic disparities amongst the ore deposits	$\delta^{34}S$: ~ +11 ± 31‰ (mostly ~ 20‰). Enriched heavy S is derived from marine sulfate. Crust with mantle mixed Pb in orogenic belts
Ore forming temperature and depth	Homogenization temperatures measured in mineral inclusions (such as hornblende) are ~80–220° with the ore forming depth being over hundreds and thousands metres	Homogenization temperatures measured in mineral inclusions (such as hornblende) are ~ 99–190° corresponding to an ore forming depth of between 0.9 and 1.38 km
Fluid characteristics	Underground thermal brine with salinity between ~10 and 30%	Thermal brine with high salinity over 5% and alkane organic matter
Relation between ore deposits and intrusion	None	None

area include a stable platform comprising an ~10-km-thick sedimentary Neoproterozoic succession, which is unconformably overlain by an ~4-km-thick succession of non-metamorphosed Early Paleozoic marine sedimentary units. The marine succession includes an ~1.8-km-thick carbonaceous succession that hosts significant Pb-Zn ore deposits.

The spatially zoned Pb-Zn deposits in the area are hosted by tectonic structures in the Early Cambrian Qingxudong Formation (Cheng et al., 2011). The host rocks include algal-reef limestone, dolomitic limestone, and calcarenite that contains bioclastics, oolitic limestone, oncolite, and carbonaceous rudite (Yang and Lao, 2007; Fu, 2011).

3.2. Conceptual models

3.2.1. Metallogenic model

The Huayuan Pb-Zn mineralisation is interpreted to be an MVT deposit related to highly enriched brines containing sulphide s flowing in structures along the edge of a large sedimentary basin (Yang, 2003; Yang and Lao, 2007; Zhong and Mao, 2007a; Table 1). The location of the mineralisation is controlled by crustal faults and by the lithochemistry of a carbonate platform facies, which is characterized by limestone and dolomitic evaporites (Zhong and Mao, 2007a). The brine was heated by an increase in temperature due to exothermal reactions

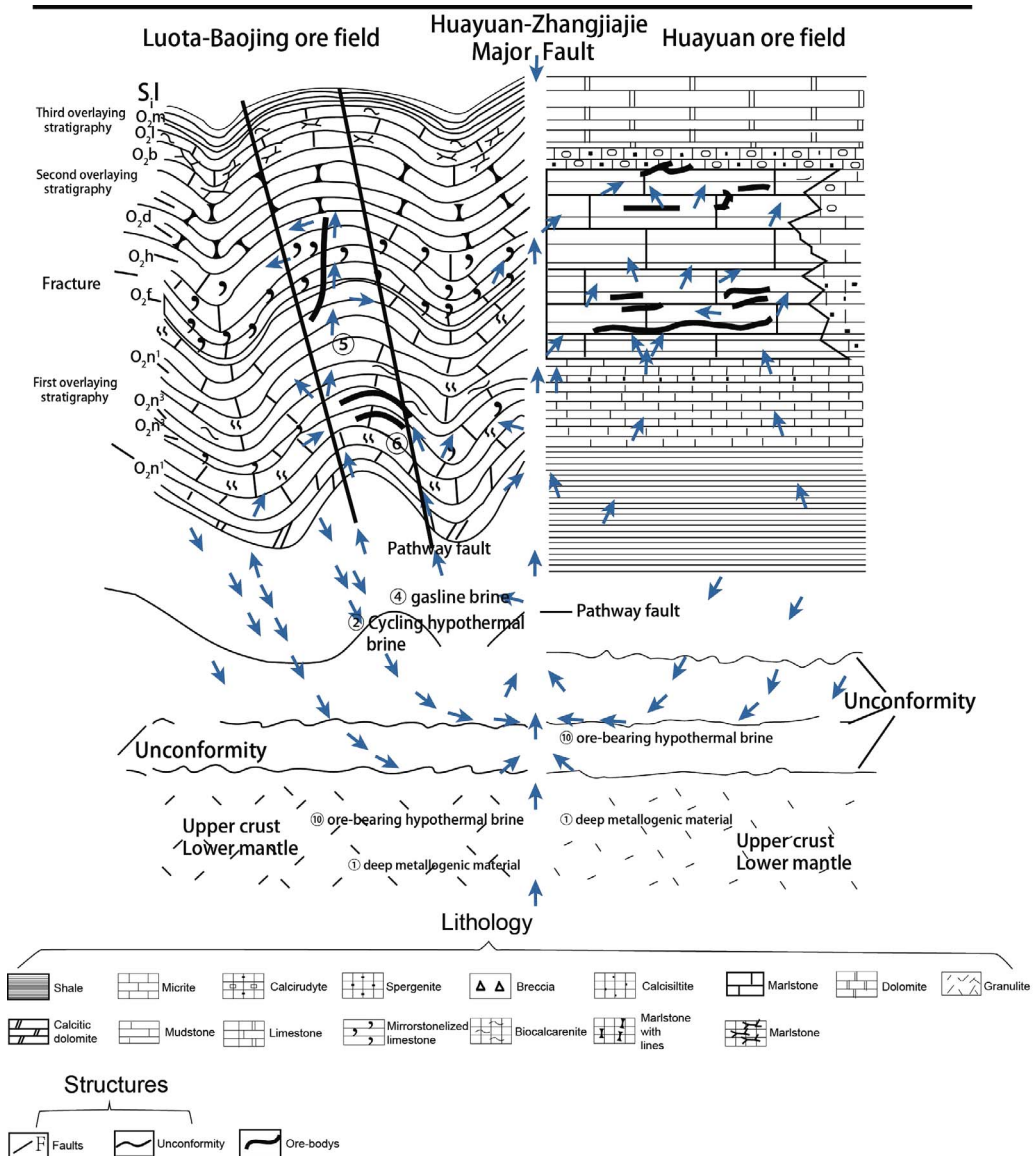

Fig. 7. Metallogenic model in Huayuan area.

associated with the reduction of asphaltenes and sulphide -forming hydrogen sulfide. Ore-forming fluids were then tectonically driven upwards, and lateral flow occurred along faults and accumulated in anticlines that were capped with impermeable barriers (or cap rocks) under which mineralisation was concentrated (Fig. 7) (Huang et al., 2011; Yang, 2003; Yang and Lao, 2007).

3.2.2. Geophysical data

No geophysical data are available for the study area, except for the 1:2,500,000-scale aeromagnetic images used to interpret the locations of major and deep-seated crustal faults (Huang et al., 2011; Yang, 2003; Chen et al., 2008). The available gravity data indicate the presence of gravity gradients dividing Hunan Province into eastern and western sections. The magnetic susceptibility of the area is weak, and the gradient of the magnetic field is small, ranging from −40 to 20 ΔT. This characteristic is interpreted to be due to the low metamorphic grade of the rocks in the area (Yang and Lao, 2007; Fu, 2011; Zhang et al., 2013).

A 1:2,500,000-scale Bouguer gravity anomaly map has also been used in this study (Fig. 8a). Negative densities generally change incrementally from southeast to northwest, and a sharp change in the gradient is present to the west of the deep-seated Zhangjiajie–Jishou Fault (Fig. 8a), which is part of the Dushan-Songtao-Dayong crustal fault. This is known as the Wuling Gravity Gradient Zone, which is ~150 km wide, extends for ~4000 km through China, and has a value of 100×10^{-5} m/s^2 from east to west (Fig. 8a; Huang et al., 2011).

The gravity field in Hunan Province has an average value of 0.85×10^{-5} m/s^2 along a NNE-trending 300-km-long gravity gradient zone that divides the province into two regions (Fig. 8a).

The magnetic data used in the study area were sourced from a 1:2,500,000-scale aeromagnetic anomaly map (Fig. 8b; Huang et al., 2011). The susceptibility values in the study area are negative, and the magnetic field is flat. Local minimum susceptibility values range from −40 to 10 ΔT, and the values in the Huayuan area are weak and characteristic of a gentle magnetic-field gradient (Fig. 8b). The trend of the magnetic field reflects the fundamental tectonic structures, with a major part of the field associated with the southeastern edge of the Yangtze Block (Fig. 8b).

3.2.3. Trap region

In Fig. 3, the trap region is composed of a fluid reservoir and fluid sink, according to the chemical system view. As discussed previously, the mineral system approach is an important methodology that considers that different sets of processes are important at different scales. In

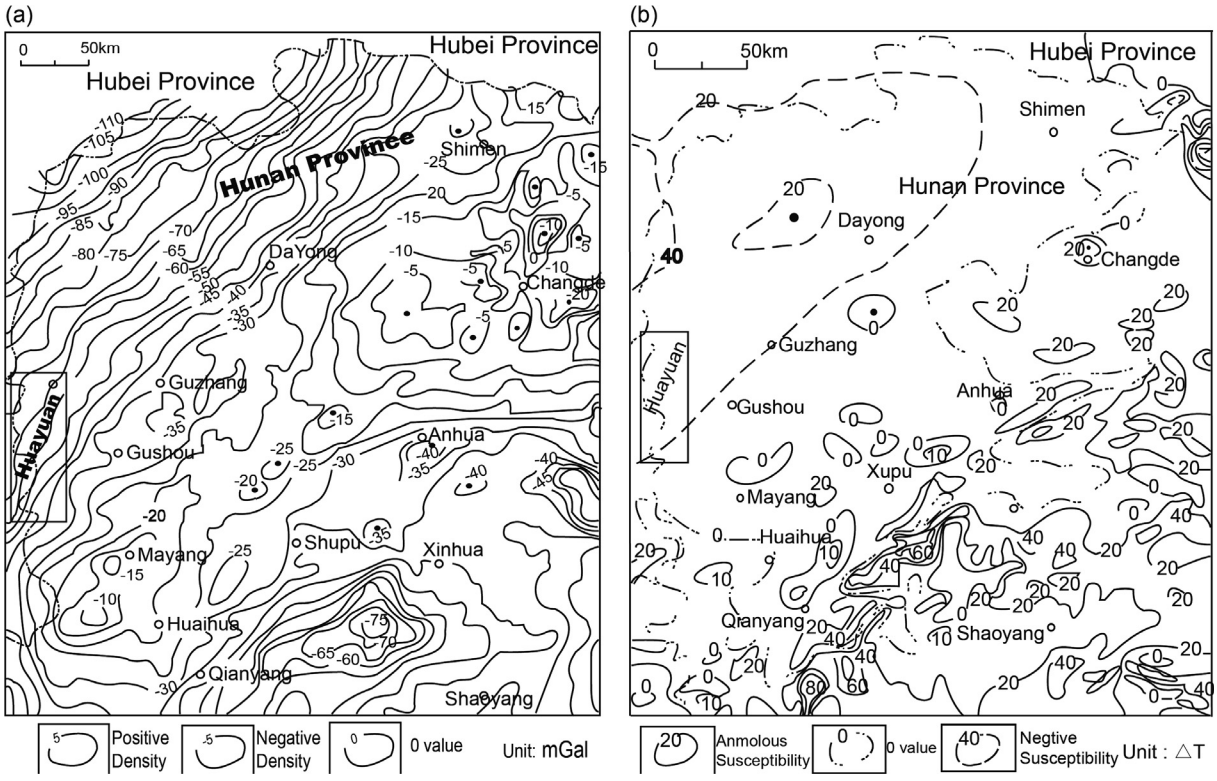

Fig. 8. Geophysic maps of the Huayuan area at a 1: 2,500,000-scale: (a) Bouguer gravity anomaly; and (b) Magnetic anomaly.

the study area, the Niutitang and Shipai formations are the source rocks, the Gaotai Formation acts as the caprock, and the Qingxudong Formation forms the ore-bearing strata, which are characteristics analogous to those of a fluid reservoir. The carbonate rocks in the Qingxudong Formation comprise algal-reef and granular limestones that are characterized by high porosity, fracture development and high permeability. The caprocks have the low porosity and permeability values that are required for the formation of a fluid reservoir (Table 2; Tang et al., 2010; Yang and Lao, 2007).

3.3. Representative mineral deposits

In this paper, the definition of a representative ore deposit is given in Section 2.2. In northwestern Hunan Province, there are three kinds of mineral deposit models, i.e., Dongjiahe-style, Limei-style, and Jiangjiaya-style. The discrimination among them are ages of ore-bearing formations. In addition, we estimated undiscovered resources of Limei-style because big resources were found in this subclass i.e. that about ten ore-deposits were found in Early Cambrian Qingxudong Formation belonging to the subclass.

The ca. 506 Ma Dongjiahe Pb-Zn deposit is located at the base of the Late Neoproterozoic Doushantuo Formation (Li, 2016). The ore-bearing horizon consists of dolomitic shale interbedded with thin layers of dolomite and carbonaceous shale at its base (Li, 2016). The mineralisation is hosted by intraformational fractures and faults in the dolomitic shale. The Zn orebodies are found in the upper part of the dolomitic shale and are associated with pyrite, whereas the Pb orebodies are located at the base of the dolomitic shale, thus forming vertical zonation. Individual orebodies are commonly layered or lenticular, and they are conformable with the surrounding rocks. The mineralisation area is approximately 150–300 m long; individual orebodies are 50–80 m long, with an average thickness of 1.4 m.

The major cross-section at the Limei Pb-Zn deposit is shown in Fig. 9. The ca. 410 Ma Limei Pb-Zn deposit contains elevated Cd and Ag assays and is hosted by algal-reef limestone in the Early Cambrian Qingxudong Formation, which is located in the NE-trending Huayuan–Chatian fold belt. The genetic environment of the ores may have been an extensional setting accompanied by the migration of ore-forming fluids through the basin (Li, 2016). The mineralisation is stratiform and forms regularly distributed NNE-trending orebodies that are up to 1575 m long, 1100 m wide, and 17 m thick, with average grades of 0.5–2.4% Pb, 0.7–5.1% Zn, and 0.03% Mo. The stratigraphically lowest orebodies have higher grades of 2–6% Pb + Zn; those at middle levels have lower grades of < 3% Pb + Zn, and those at the highest stratigraphic levels have grades that fall between these values. The orebodies in the northern part of the mining area are richer in Zn and poorer in Pb. The Zn grade decreases from north to south, whereas the Pb grade increases. The Pb:Zn ratio is approximately 10:1 in the north and 2:1 in the south.

The ca. 372 Ma Jiangjiaya Pb-Zn deposit is hosted by the Early Ordovician Tongzi Formation in faults that acted as conduits for mineralised fluids in the basin (Li, 2016). The orebodies in the area extend from Zhangjiapo in the west to Labache in the east, forming a mineralised zone that is approximately 3 km long and 300 m wide, with several outcrops of silicified limestone exposed along the mineralisation zone. The orebodies are lensoidal, nest-shaped, stratiform, and veined. The smaller orebodies are < 2 m long and < 0.5 m thick. The larger orebodies are approximately 10 m long and up to 2 m thick. There are four veins that are longer than 100 m in this area. The longest is 550 m, with a trend of ~45° and a dip of ~ 70°, which is subparallel to the bedding of the host rocks. The grade of the mineralisation decreases from west to east; in the western part of the area, the mineralisation is richer in galena, whereas that in the central part is richer in sphalerite.

The characteristic features of the descriptive model, mineral system, and typical deposit model are listed in Table 3; these data were used to calculate the similarity coefficient in Section 4.6.

Table 2
Mineral system in North-western Hunan area at regional scale.

Commodity	Critical mineral systems component											
	Source		Active pathway			Trap				Chemical scrubber		
	Targeting element	Primary data	Predictor map	Targeting element	Primary data	Predictor map	Physical throttle			Targeting element	Primary data	Predictor map
							Targeting element	Primary data	Predictor map			
MVT Pb-Zn deposits	Cambrian Niutitang to Shipai Formation (which carry Pb and Zn elements)	Geological mapping	Cambrian Niutitang to Shipai Formation	Deep faults	Structural interpretation	Distance to deep faults in study area	Cambrian Qingxudong Formation	Geolog-ical mappin-g	Cambrian Qingxud-ong Formation	Reduced Stratigra-phy	Geoch-emistry	Lead, zinc, and related elements anomalies
						Density map of deep faults						Combination of geochemical anomaly

4. Mineral resources assessment

4.1. Datasets

Spatial datasets were collected on the regional scale of northwestern Hunan Province, and higher-resolution datasets were collected in Huayuan district. The regional dataset included topographic data, a 1:200,000-scale geological map, a 1:200,000-scale ore deposits map, and 1:200,000-scale regional stream sediment data. The district-scale dataset included 1:50,000-scale geological maps, deep drillhole data, and Geological Survey and exploration reports of typical deposits in Huayuan district (Table 4; Huang et al., 2011; Zhang et al., 2013). The aim of the study is to estimate mineral resources in Huayuan district.

4.2. Coordinate systems

The level of detail of the data in Hunan Province depends on different coordinate systems. This necessitates the processing of maps with latitude and longitude coordinate systems at different scales, such as Gauss–Kruger projections, which use a central meridian (depending on the range of longitudes and latitudes of the province within a 3° span), Krasovsky ellipsoid, the Beijing 54 coordinate system, and geodetic coordinates converted from latitude and longitude coordinates using ArcGIS and MapGIS.

The final coordinates in the study area are: (i) Hunan Province, which ranges from 108°47′ to 114°15′E and 24°38′ to 30°08′N, 109°15′ to 111°00′E; (ii) northwestern Hunan region, which ranges from 109°15′ to 111°00′E and 28°00′ to 30°00′N; and (iii) 109°15′ to 109°30′E and 28°30′ to 28°40′N. The representative Limei deposit in the study area ranges from 109°21′19″ to 109°22′38″E and 28°31′03″ to 28°31′41″N. A GIS-based map with unified coordinates is presented as a mineral potential map in Fig. 10.

4.3. Geological observations

Geological observations and descriptions are not always uniform between the different scales presented, due to the degree of detail of the data at a given scale. Differences in detail require standardization before prospectivity maps can be compiled. An example of this is the MVT Pb-Zn mineralisation in the Qingxudong Formation, as discussed in Section 3. Local geologists have described the geology at different scales and have thus applied different rock type names (e.g., dolomite, limestone, and argillaceous limestone), as shown in Fig. 10.

4.4. Delineation of traps

4.4.1. Regional scale

As mentioned in Section 2.3.1, the GIS-based prospectivity mapping method was used to delineate traps where mineralisation may be present. To combine multiple 2D spatial datasets to mark the boundaries of probable traps, BoostWoE is used in this section as an aid to delineate traps of undiscovered MVT Pb-Zn resources at Huayuan. Finally, the resultant BoostWofEs are shown in Tables 5 and 6.

During the above process, a critical feature for prospectivity mapping at Huayuan is the processing of geochemical data (c.f. Section 3). Because the mineralisation process represents multiple stages and multiple sources, geochemical elements usually exhibit spatially complex paragenetic relationships (Singer and Kouda, 2001; Tripathi, 1979; Voroshilov, 2009; Huang et al., 2011). It is thus important to choose an appropriate method to extract and thoroughly analyse integrated geochemical data. The partial least squares (PLS) method is used in this manuscript to identify integrated geochemical anomalies. The PLS method can analyse data containing both multi-independent and multi-dependent variables by extracting the main components. In this study, we collected 1:200,000-scale stream sediment datasets. Twenty-two trace elements in the study area were measured as the independent

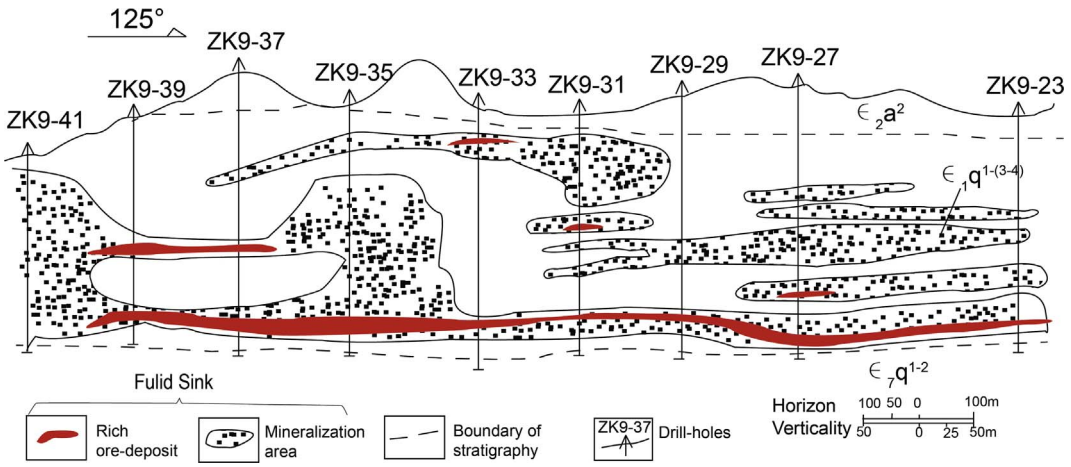

Fig. 9. Cross-section of the Limei typical ore-deposit (modified after Fu, 2011).

Table 3
Descriptive MVT Pb-Zn mineral deposit.

Favorable Features	MVT Pb-Zn mineral deposit	Pb-Zn predictor in Limei
Sedimentary strata (which carry metal ions trapped within day and phyllosilicate minerals and electrochemically absorbed to their surfaces	Sedimentary strata	Niutitang Formation
Alteration features	Organic matter mineralization, silicification, clayization, micacization, feldspathization Remote sensing interpretation alteration	Baratization, calcilization, pyritization, dolomitization
Structural interpretation	Crustal fault Remote sensing interpretation fault	Dushan-Songtao-Dayong deep fault, a part of it named Zhangjiajie-Huayuan fault
The mineralization is believed to be syngenetic to early diagenetic, deposited contemporaneously with or shortly after the host rocks	Breccias or breccia density map	
Ore-bearing formation	Carbonate formation	Dolomite or limestone in Qingxudong formation
Geochemistry	Pb, Zn, As, Sb content maps	Pb, Zn, Cd content maps
Lithofacies paleogeography	Reef, backbarrier deposit	Algal reef facies
Native concentrate anomaly	Pb, Zn anomaly	

variable data set 'X', including Ag, As, Au, Ba, Bi, Cd, Cr, Cu, Hg, Mn, Mo, Nb, Ni, Pb, Sb, Sn, Sr, Ti, V, W, Zn, and Zr. Zinc, which is the major ore-forming element, was selected as a dependent variable in data set 'Y' (Wold et al., 1984; Lorber et al., 1987). After calculation using the PLS method, five principal components known as *Factors 1–5* were calculated. Statistically, the first component contains the most important information for the whole system, which best helps explain the dependent variable 'Y'. The values of the first component are processed by Kriging interpolation calculations, and the integrated anomalies are extracted as shown in Fig. 11. To verify this decision, the cross-in-validation of the five components was processed. The Predicted Error Sum of Squares (PRESS) and cross-validation variable (Q2) of each component was calculated using the ANAGRA software package (Table. 7 and Fig. 11 h). The Q2 value should be larger than 0.0975 (Wang, 1999; Boulesteix, 2004). Based on the above analysis, the Factor4 and Factor5 values of principal components were deleted.

Points were then calculated by BoostsWofE, and inflection points are present where the Similarity Index appears on the accumulation graph (Fig. 12(c)). Thus, the classification thresholds {0.95, 0.8, 0.6} were chosen based on the accumulation graph; these results are shown in Table 5 and Fig. 12(a).

According to the mineral potential map Fig. 12 (b), favourable feature layers. such as the PLS geochemical anomaly, Pb and Zn anomalies, Qingxudong Formation, and structures, are synthetically

Table 4
Geological Survey data from the Huayuan district.

Data set type	Scale	Description of the data	Source
Details of original multi-type data in Huayuan district			
Regional scale dataset			
Regional geological map in North-western Hunan province	1:200,000		
Geochemical stream sediment data	1:200,000	Span of sample points is 2 km; The elements include Ag, As, Au, B, Ba, Be, Bi, Cd, Cr, Cu, F, Hg, Li, Mn, Mo, Nb, Ni, P, Pb, Sb, Sn, Ti, V, W, Zn, Zr, Al_2O_3, CaO, Fe_2O_3, K_2O, MgO, Na_2O, SiO_2.	
District scale datasets			
Huayuan Geological Map	1:50,000	1 map covered the Huayuan study district including stratigraphy boundary, orientations, stratigraphic column, and structures.	Zhang et al. (2013)
Ancient structure and sedimentary litho-facis map	1:50,000	1 map covered Huayuan-Malichang study district including ancient sedimentary litho-faces and structures.	Xue (2015)

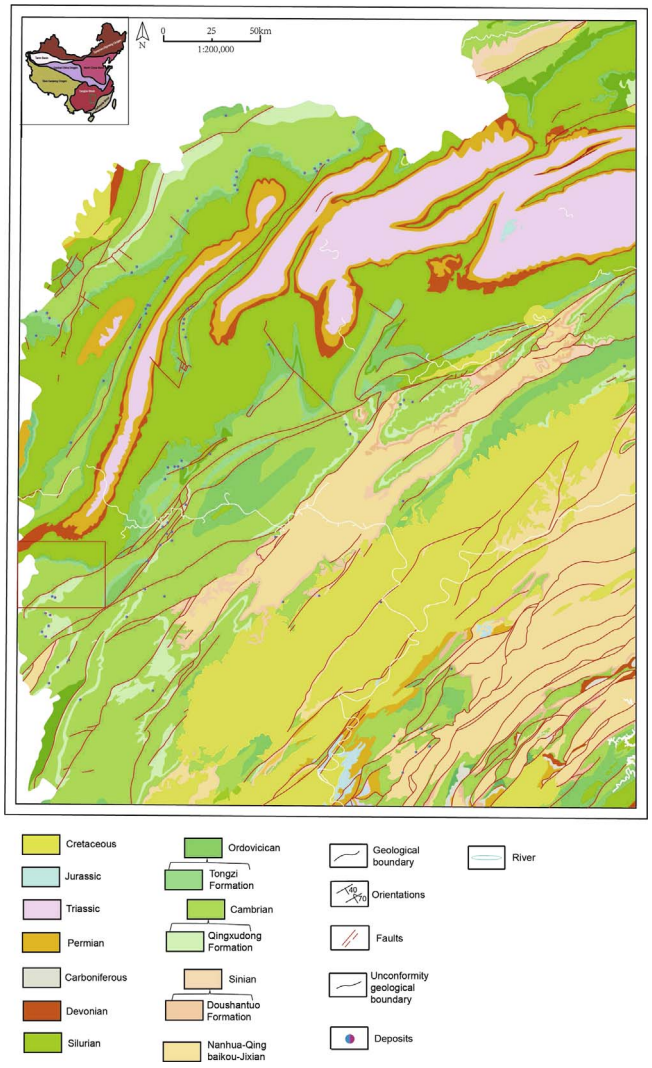

Fig. 10. Regional geological map (modified after Zhang et al., 2013).

Table 5
Results of classification at regional scale.

Classification	A	B	C	Others
Value	[1, 0.95]	[0.95, 0.8]	[0.8, 0.6]	[0.6, 0]

interpreted to delineate the range of traps in the mineral system. A metallogenic prediction (Xue, 2015) was carried out based on the lithofacies distribution of the Cambrian unit and the Huayuan-zhangjiajie coeval fault. It was verified that the ore-bearing algal limestone facies exhibits a NE-NEE distribution and crosses the Huayuan-zhangjiajie Fault, as determined from drilling that revealed concealed deposits at Yangjiazhai and Danaopo. In addition, deposits were discovered at depths of 600 m in the north and 100 m in the south of the Huayuan-zhangjiajie Fault. Thus, we conclude that the northern hanging wall of the Huayuan-zhangjiajie Fault has dropped ~500 m. It can therefore be concluded that the Huayuan-zhangjiajie Fault does not represent the northern border of the ore field but has instead rearranged the mineralisation. Based on the above description, the trap was delineated by the dashed purple line in Fig. 12(a).

Table 6
Results of Boost weights of evidences at regional scale.

Evidence Names	W^+	W^-	C
Cd	1.33727	-0.11692	1.45419
Pb	1.70052	0	1.70052
Zn	1.72216	0	1.72216
Qingxudong formation	2.94143	0	2.94143
Entropy anomaly of geological formation	0.46734	−0.21902	0.68636
Fault buffer (1 km)	0.50548	0	0.50548
Fault density	0.61858	−1.195883	1.814463
Buffer of structure buffer from remote sensing (1.5 km)	1.01502	−0.49323	1.50825
Heavy mineral anomaly of Pb and Zn	1.63342	−0.59041	2.22383
Integrated heavy mineral anomaly PLS	0.68818	0	0.68818

4.4.2. District scale

As mentioned in Section 2.3.1, the traps delineated using regional-scale datasets can be refined using highly accurate maps at the district scale.

The Pb-Zn deposits in the study area are stratabound and hosted by the Qingxudong Formation. The mineralisation is controlled by NE-trending structures and the algal limestone strata towards the base of the formation. The sedimentary facies of this region have been influenced by early structures affecting the $\epsilon_2 q$ unit, including folding, which resulted in dilatational zones creating space in which minerals could be deposited. Additionally, the interlayer breccia and carbonate were deposited, which resulted in the accumulation of ore in dilatational zones. The algal reef lithofacies at the base of the Qingxudong Formation is an important potential host for mineralisation.

The lithofacies paleogeographic map was compiled to understand the sedimentary facies and tectonic evolution in Limei-Malicahng district, northwestern Hunan Province, China. This study used a 1:50,000-scale lithofacies palaeogeographic map for the Huayuan-Malichang district (Fig. 13; Xue, 2015). The map was compiled using single factor analysis and the independent factors comprehensive mapping method proposed by Feng (2004), which includes three steps. The first step is the recognition of major rocks and lithofacies based on the construction of cross-sections by geologists at the study district. The second step involves a single factor, such as the thicknesses of stratigraphic units, and the proportion of rock types is determined based on the analysis of measured cross-sections and drillholes so that the factor independently reflects the sedimentary environment in the study area. These data are then compiled as a contour map. Finally, the lithofacies palaeogeographic map is compiled using a combination of contour maps, petrology, and sedimentary facies (Feng, 1986, 2004; Feng et al., 1999).

The GIS-based approach was used in this study to refine the trap delineated at a regional scale by integrating the algal reef lithofacies, structures, and Qingxudong Formation at a district scale. Unfortunately, we did not collect 1:50,000-scale stream sediment data; thus, we still had to use the 1:200,000-scale map on the district scale. The cells were reorganized as 500 m × 500 m, and we integrated the 1:50,000-scale Qingxudong Formation, 1:50,000-scale faults layer, 1:50,000-scale algal reef lithofacies map, and geochemical anomalies extracted from the 1:200,000 map into a single possibility map by BoostWofEs. A new layer was extracted as the refined trap, which is shown as the yellow line in Fig. 14. As in Fig. 12, the inflexions in cumulative probability used to divide the data into classes A, B, and C are 0.95, 0.85, and 0.6, respectively, as shown in Fig. 14(c).

In general, the trap boundaries on the district scale are composed of an ore-bearing formation and an algal reef facies. The spatial shape of the trap is same as the trends defined by the Qingxudong Formation and structures such as faults and folds.

4.5. Volume of trap (Fluid Reservoir)

The trap was seen as a regular 3D geometric model in Part 1, which means that its volume can be calculated by multiplying its area in 2D by its depth. The depth is an empirical value obtained from representative deposits. In Table 8, the depth of the representative Limei deposit is

(a) Proportion of Variance Explained (Percentage)

-	Input variables (X)		Target Variables (Y)	
Latent Factor	Current X (%)	Cumulative X (%)	Current Y (%)	Cumulative Y (%)
Factor1	20.21	20.21	62.104	62.104
Factor2	10.894	31.105	26.969	89.073
Factor3	4.345	35.449	8.046	97.118
Factor4	9.48	44.93	1.742	98.86
Factor5	5.998	50.928	0.796	99.656

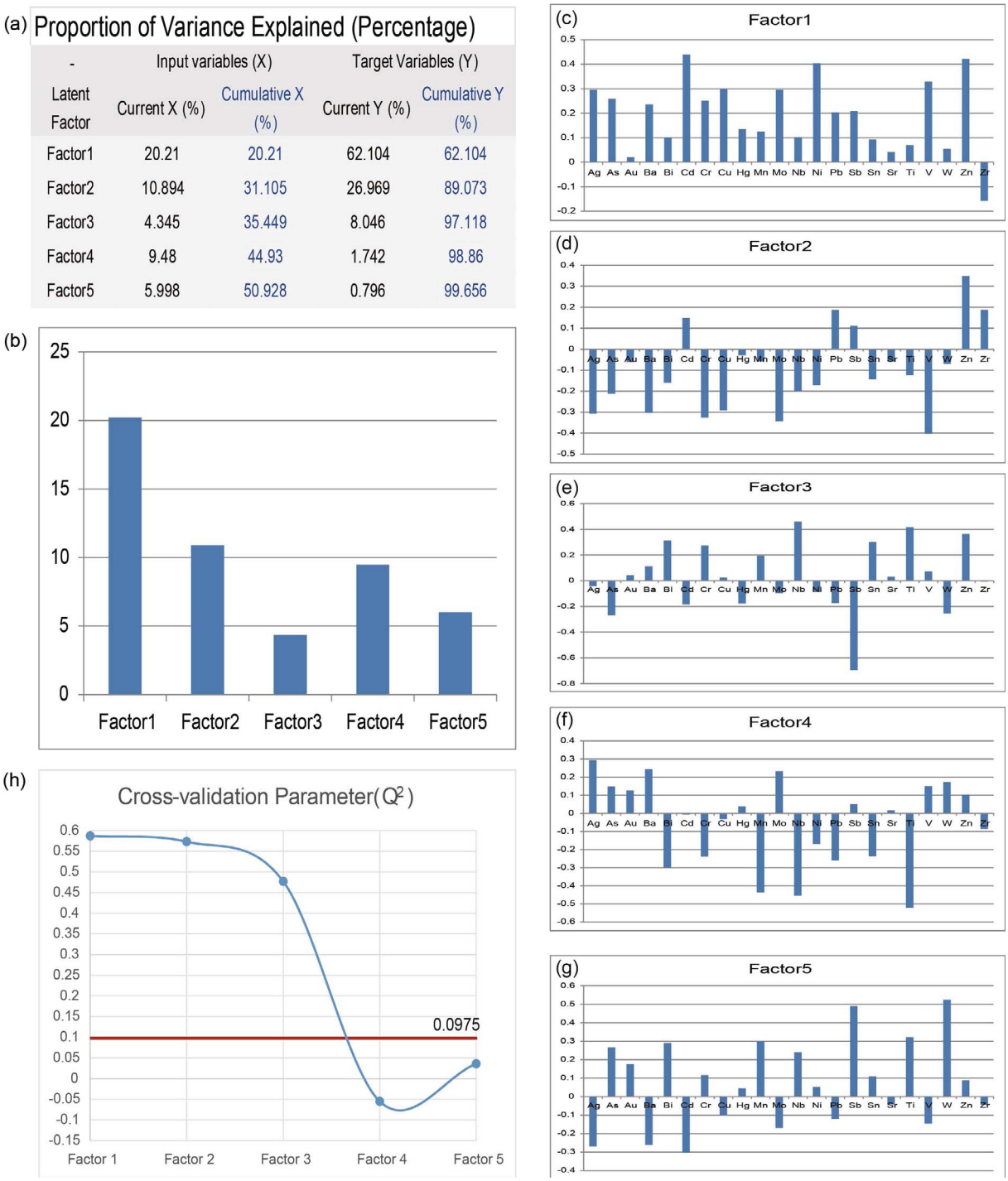

Fig. 11. PLS method to integrate geochemical anomaly (modified after Wang et al., 2017 under review) with: (a) Proportion of factors; (b) Main factors comparison; (c) Elements associations of factor1; (d) Elements associations of factor2; (d) Elements associations of factor3; (e) Elements associations of factor4; (f) Elements associations of factor5; and (h) Cross-invalidation of components of geochemical data.

Table 7
Cross-invalidation of components.

H number of components	Q^2 cross-validation parameter	PRESS prediction residual error sum of squares	D(PRESS)
1	0.587	148,330,608	58.70%
2	0.573	58,066,876	60.90%
3	0.477	20,507,252	64.70%
4	-0.055	10,913,554	46.80%

210 m. Thus, the volume of the trap in the Huayuan district is equal to 1.09266×10^9 m^3 using Eq. (8). In Part II, we construct 3D models of the Qingxudong Formation and crustal structures; then, we use Eq. (9) to improve Fig. 17.

4.6. Similarity Index

Limei is a typical MVT deposit in the Huayuan district; the trap in which the deposit is located is delineated in Section 4.4 and Fig. 14 inside the same mineral system. Here, we use two methods, i.e.,

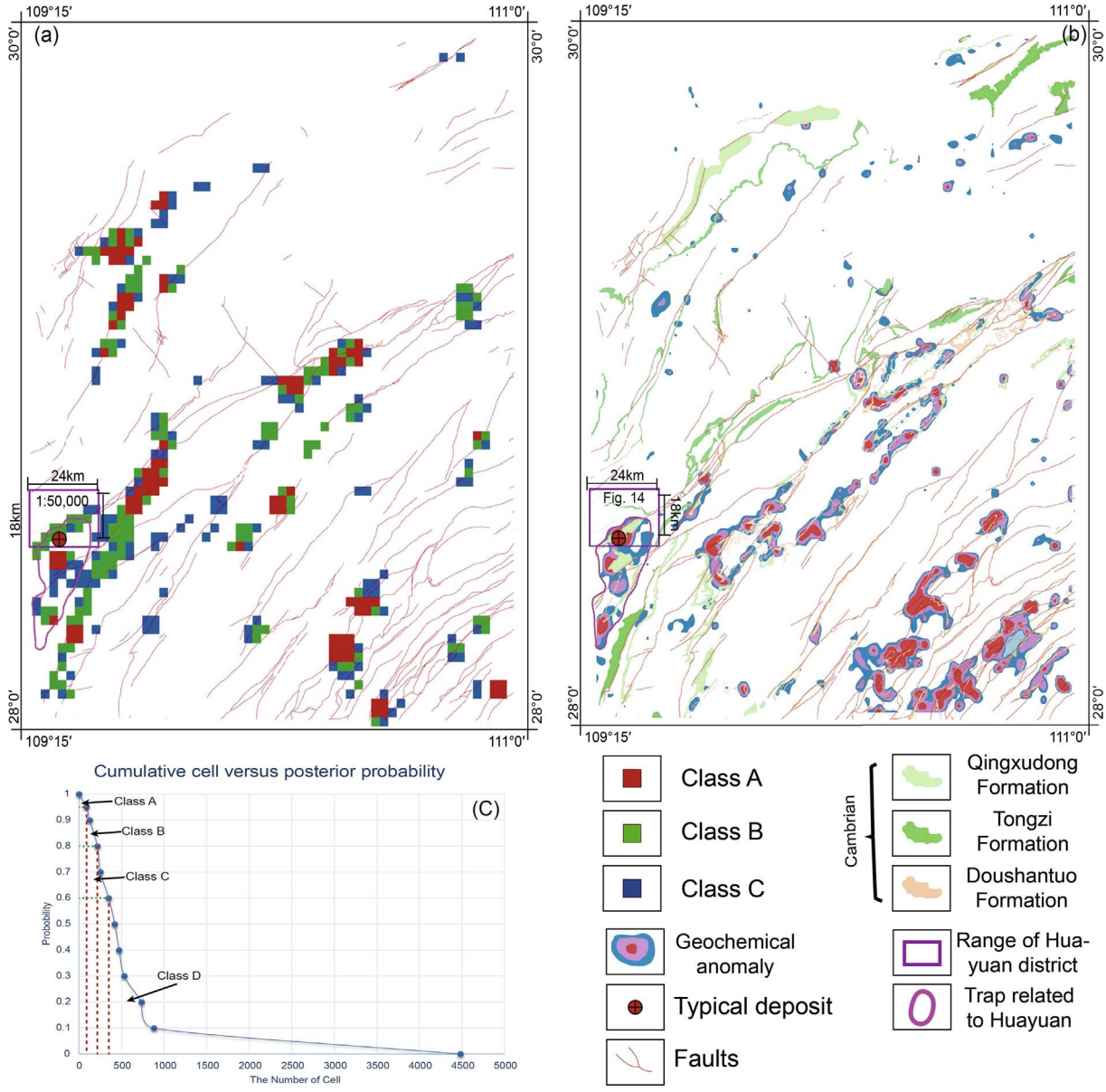

Fig. 12. Delineated traps at regional scale based on GIS-based prospectivity mapping: (a) Colourful blocks map; (b) With various favourable features used; and (c) Cumulative probability map.

BoostWofE and the Jarcard Index, as presented in Section 2.4. The variable S_{trap} is a weighted mean method based on all S_{icell} values from the cells in the Huayuan district.

As in Fig. 14, a total of 333 cells in the mineral potential map established by BoostWofEs were extracted because the posterior possibility is larger than 0.6, which is the threshold of class C.

We also use the Jarcard Index to calculate the similarity coefficient between the descriptive models, reference mineral deposit, and cells in the trap and Huayuan district. The favourable features of a descriptive model are shown in Table 3, where they are digitalized as a vector {1, 1, 1, 1, 1} that contains favourable ore-bearing formation, geochemical anomaly (including Pb, Zn, Cd, and PLC) data; the favourable features in the Limei reference deposit are given the same value {1, 1, 1, 1, 1} based on the exploration report, and the calculated values in the cells are shown in Fig. 14, except for those in the posterior of the field. The Similarity Index in the trap is the weighted mean value based on each cell calculated using Eq. (8).

4.7. Ore-bearing ratio

As defined in Section 2.5, the ore-bearing ratio is equal to the arithmetic mean based on Table 8. The Hunan Bureau of Geology and Mineral Resources has discovered several important Pb-Zn deposits in the Huayuan-Malichang area, including Limei, Naizibao, Bamaozhai, Tudiping, Yutangzhai, Danaopo, Baiyan, and Qingshuitang. However, we only collected data from three mineral exploration and resource reports, i.e., those of the Limei, Nazibao, and Yutangzhai deposits, because the reports from other deposits did not provide or could not infer the volumes of ore-bearing zones. The ore-bearing ratio in the Huayuan district is defined as follows:

$$\text{Ore-bearing ratio}_{Pb}\frac{\frac{16476.6}{1.82\times10^{8}}+\frac{3615}{1.12\times10^{8}}+\frac{11037}{1.38\times10^{8}}}{3}=6.75910^{-5}$$

$$\text{Ore-bearing ratio}_{Zn}=\frac{\frac{1837885.78}{1.82\times10^{8}}+\frac{102708}{1.12\times10^{8}}+\frac{18169}{1.38\times10^{8}}}{3}=3.71610^{-3}$$

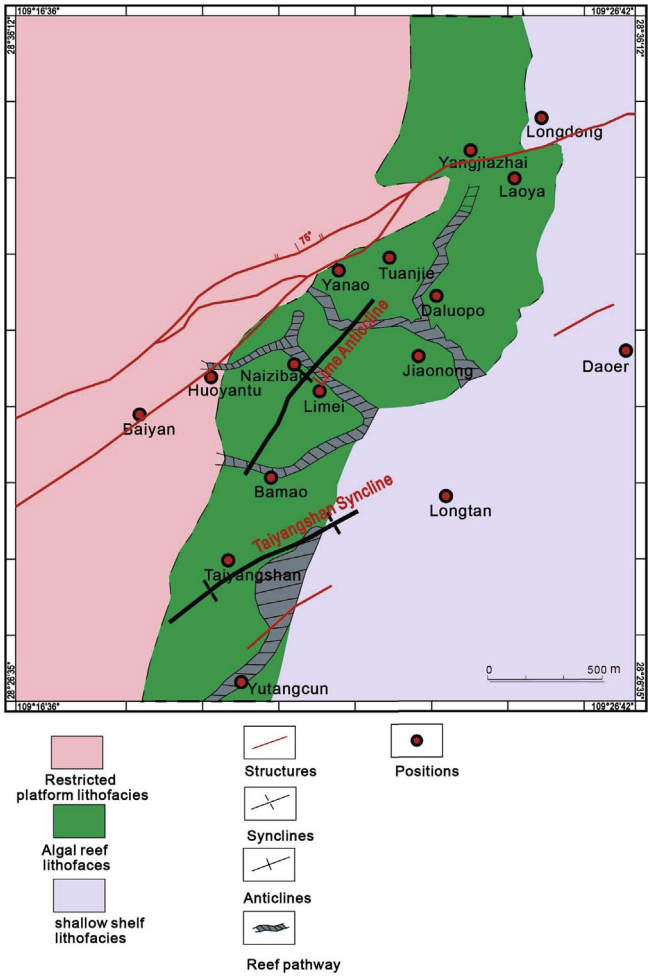

Fig. 13. Structure and sedimentary lithofacies palaeogeographic map of the Huayuan-Malichang district.

4.8. Estimation of resources

Following the above procedure, the Similarity Index S, the ore-bearing ratio ($C_{ore-bearing}$), and the volume of the trap (V_{trap}) are calculated, and Eq. (7) is used to estimate the undiscovered mineral resources in the Huayuan district as follows.

If the posterior from the WofE method is used:

$$W_{Pb,resources} = \sum_{i=0}^{333} 125m \times 125m \times s_i \times 6.759 \times 10^{-5} = 63{,}531t;$$

$$W_{Zn,resources} = \sum_{i=0}^{333} 125m \times 125m \times s_i \times 3.716 \times 10^{-3} = = 3{,}667{,}509t.$$

where s_i is posterior in cell i.

If the similarity coefficient from the Jarcard Index method is used:

$$W_{Pb,resources} = \sum_{i=0}^{333} 125 \times 125 \times s_i \times 6.759 \times 10^{-5} = 79{,}231t;$$

$$W_{Zn,resources} = \sum_{i=0}^{333} 125 \times 125 \times s_i \times 3.716 \times 10^{-3} = 4{,}573{,}836t.$$

where s_i is the Jarcard Index in cell i.

5. Discussion

5.1. Geological perspective

In this study, the Pb-Zn deposits located in the algal-reef limestone of the Cambrian Qingxudong Formation in the Huyuan district were examined in Fig. 14. The distribution of these orebodies is strictly controlled by the lithology and depositional age, and the Pb-Zn deposits in the area are stratiform in nature. The major mineralising fluids were sourced from the crust and upper mantle and were mobilised during the Dushan-Songtao-Dayong tectonic events (Xue, 2015); the Zhangjiajie-Huayuan fault formed later than the mineralisation and broke the MVT Pb-Zn orebodies in the study area. Mineralised fluids were deposited in the algal-reef limestone, dolomitized limestone, and calcarenite of the Qingxudong Formation. The limestone is characterized by high porosity, fracture development and high permeability.

Important progress has been made in estimating the resources of the Huyuan-Fenghuang region (northwestern Hunan Province) over the last 10 years. The current estimate is > 20 Mt (Yuan, 2013). Furthermore, almost all of the deposits in the Huyuan-Fenghuang region are located in the Huayuan area (Huang et al., 2011; Li, 2016). Thus, the estimated resources at the camp scale represent an acceptable result, as is shown in Section 4.8. There are several areas, however, that could be investigated and improved in the future. The first issue is that according to mineral genesis and deposit models, there appear to be several types of deposits (e.g., Cox and Singer, 1986). Specifically, these examples include mixed volcanic- and sedimentary-hosted deposits; volcanic hydrothermal deposits; magmatic deposits; porphyry and skarn deposits; sedimentary metamorphic deposits; stratabound deposits; and, finally, gold in shear zones or metamorphic diamictite. In all deposits, except for sedimentary-hosted deposits, it is more difficult to convert geological models to 3D proxies than it is in stratabound deposits. The second issue is that only one typical deposit was used to calculate the Similarity Index. Other ore deposits of the same type will be examined in the future in order to improve the Similarity Index. The third issue is that this Pb-Zn mineralisation was deposited over a long period of time, i.e., from the Neoproterozoic to Ordovician; although the algae-reef limestone is important, we lack 3D models of it.

5.2. Calculation of variables

The Similarity Index, ore-bearing ratio (C_i), and volume of the trap (V_{trap}) are discussed below.

5.2.1. Similarity Index

The Similarity Index inside a target is a weighted mean method based on all permissive cells in 2D; it is calculated using the BoostWofE and Jarcard methods. Although this is an expedient method, obviously, the use of 3D models such as voxels is more accurate. Before using voxel-models, it is difficult to collect enough data in many study areas to construct accurate 3D models at a district scale. If a 3D dataset is available, it could be used to infer the models of ore-bearing formations, ore-controlling structures, and other favourable features based on the analysis of a mineral system and a descriptive deposit model.

5.2.2. Ore-bearing ratio

The ore-bearing ratio is calculated in this study by correlation; the trend analysis method is based on the analysis of representative deposits in a study area, as outlined in Sections 2.5 and 4.7. The result depends on the area (S) of the polygons of ore-bearing zones on the ore deposit scale and the estimated depth (H) determined from a drillhole at the same deposit. However, this becomes difficult when the distribution of ore-bearing zones is complicated. An accurate ore-bearing ratio can be calculated based on the volume (V) of the 3D geometry of ore-bearing zones (known as a fluid sink). Numerous packages, such as Micromine and Surpac, can implement 3D geological modelling at the

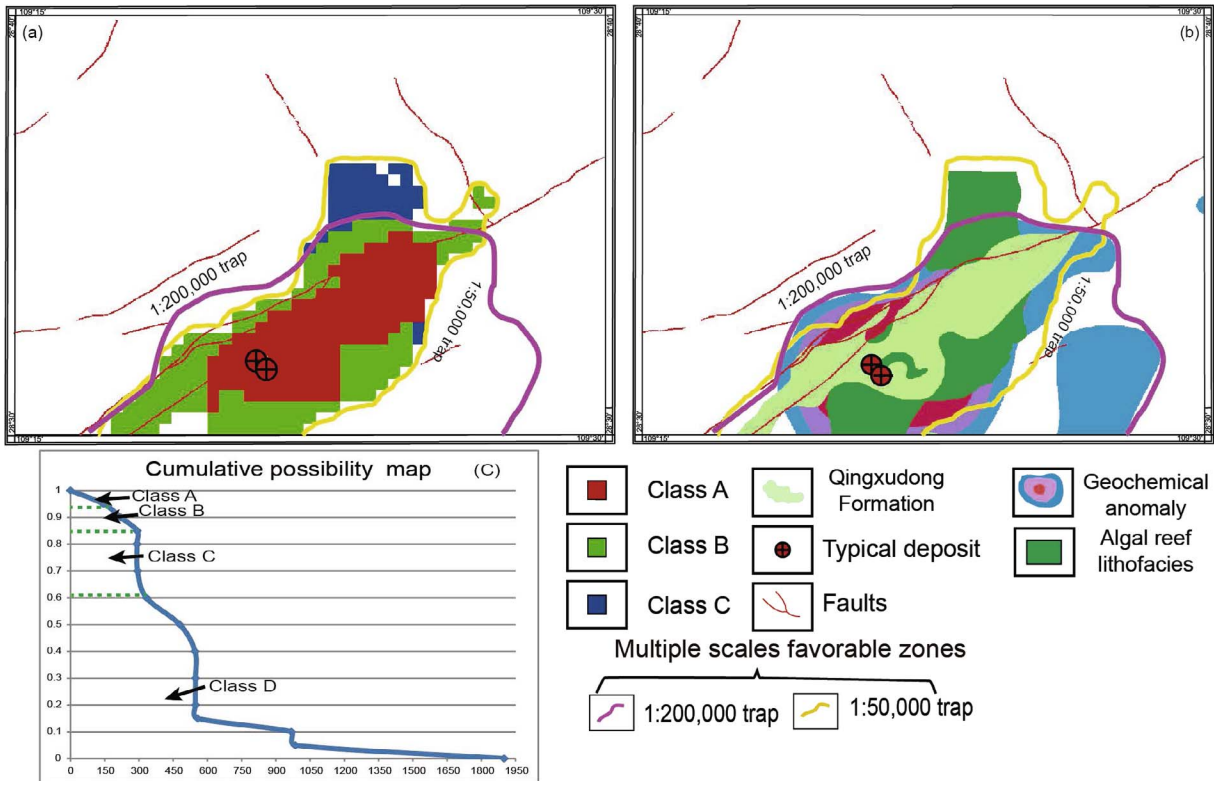

Fig. 14. Refined permissive boundary of the trap in the Huayuan district: (a). Colourful blocks map; (b) With various favourable features used; and (c) Cumulative probability map.

Table 8
Representative MVT Pb-Zn deposits in the Huayuan district in the same mineral system.

Deposit names	Pb resources (t)	Zn resources (t)	Volume (km^3)	Sub-type	Ore-bearing formation
Limei	16476.6	1837885.78	0.182	Limei-style	Middle unit in Qingxudong formation
Naizibao	3615	102,708	0.112	Limei-style	Middle unit in Qingxudong formation
Yutangzhai	11,037	18,169	0.138	Limei-style	Middle unit in Qingxudong formation

ore deposit scale. In these packages, geological surfaces are restructured based on cross-sections that are defined according to an exploration dataset, after which the surface is drawn based on a user knowledge base.

5.2.3. Three-dimensional geological modelling

In prospectivity mapping, an unresolved issue is that predictive proxies are two-dimensional GIS layers at a regional scale, whereas mineralising processes occur in four dimensions (i.e., space and time). This is a critical reason why the quantitative estimates of undiscovered resources based on widely spaced regional datasets are usually not accepted as exploration targets at camp and larger scales. Obviously, 3D geometric models more closely represent mineral systems in reality, but acquiring 3D data at a camp or regional scale is difficult. One way of overcoming the lack of 3D data at a camp scale is to use 3D geophysical modelling techniques, such as forward modelling or inversion models, to develop 3D geological models (Joly et al., 2012; Perrouty et al., 2014; Wang et al., 2015). However, this method is limited by: (i) the inability to distinguish between the physical properties of different types of mineralisation and ore-bearing formations; (ii) the fact that 3D geophysical modelling techniques depend on the quality of the geophysical data and how well geological characteristics are recognized; and (iii) the cost of measuring high-resolution (1:50,000-scale) geophysical data. Early 3D prospectivity mapping efforts relied on a series of stacked geologic sections interpreted from field studies. With the development of 3D modelling, geologists can construct geological models based on geological survey datasets. Camp-scale or district-scale datasets generally include geological descriptions, orientations, stratigraphic columns, interpretative cross-sections, deep drillhole data, and petrophysical and geophysical data. Based on such datasets, 3D modelling processes can also be used to construct geological models using implicit modelling software (Geomodeller) or explicit modelling software (GeoCAD).

Currently, a popular process is to generate 3D mineral potential maps and estimate the mineral resources at a camp or district scale (Fig. 15) rather than a regional scale. The reasons for this are that (i) regional-scale datasets are too “rough” or “vague” to be useful for assessments of buried mineralisation; and (ii) the size of the regional scale is too “big” for a geological survey to be cost-effective. However, mineralisation is fractal in nature, as it forms at multiple scales, which is why conceptual mineral system models have been developed for exploration (Fig. 3; Wyborn et al., 1994; Hronsky and Groves, 2008; McCuaig and Hronsky, 2014; Hagemann et al., 2016).

Although 3D geometric models have several technical issues, they are very useful for improving the accuracy of variables, such as the ore-bearing ratio, and volume calculations. Currently, explicit and implicit methods are the major methods of 3D modelling. These two methods can be applied to different kinds of situations. The explicit method is suitable for datasets with little uncertainty, such as those including tens of boreholes in a mine. However, the disadvantages of the explicit method are that geologists must spend a lot of time compiling cross-sections and connecting boundaries, and they cannot update the models when they are constructed. For a study area with a spare deep dataset or poor knowledge, such as a green field, the implicit method is more

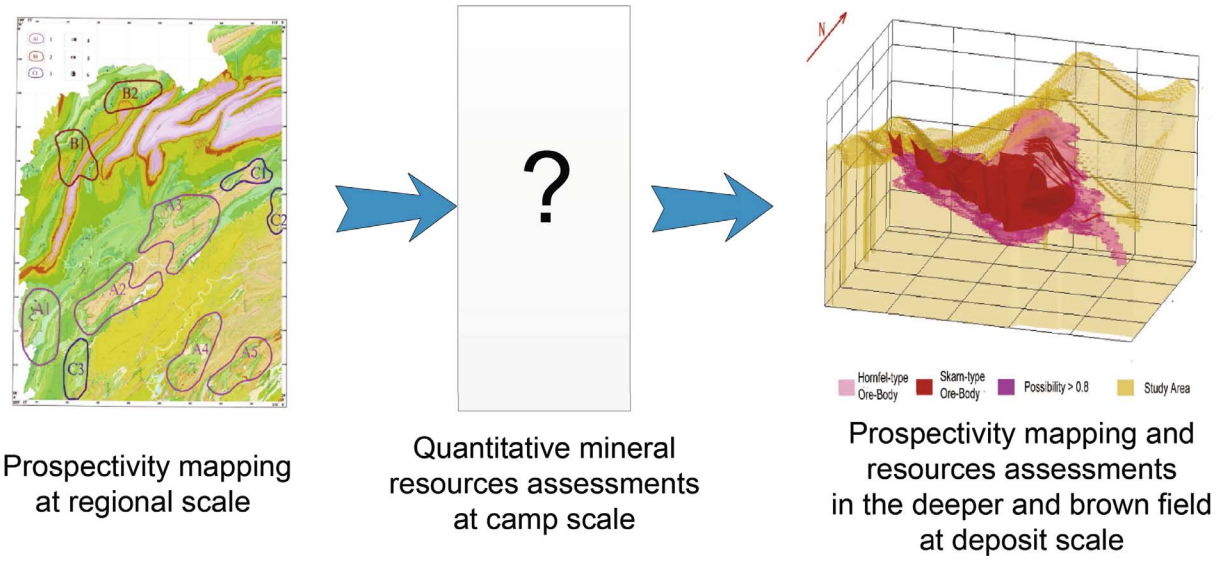

Fig. 15. What studies of prospectivity mapping are and how to calculate undiscovered resource assessment at district scale.

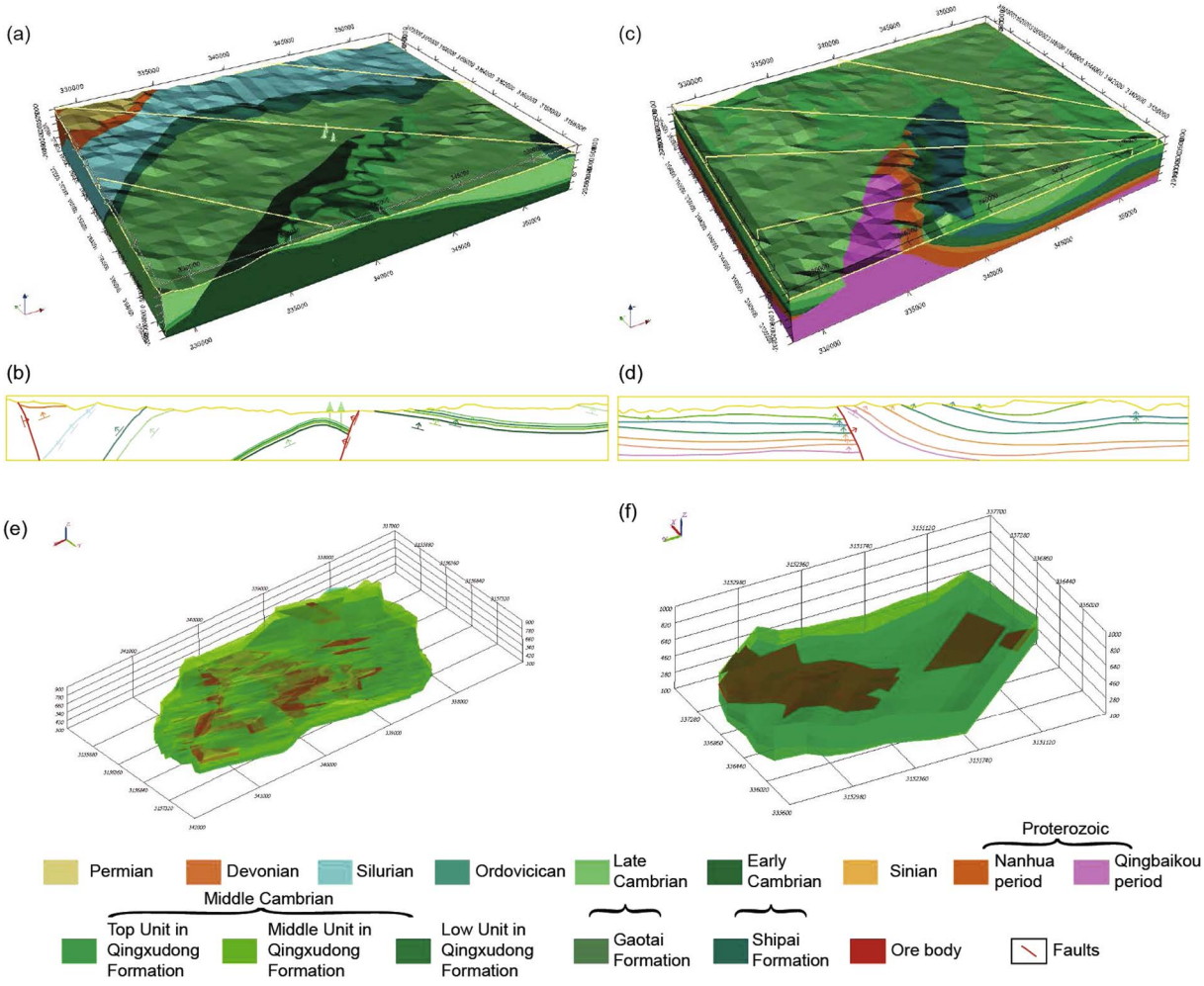

Fig. 16. 3D geological models in Part II. (a) Huayuan district model; (b) Main cross-section in Huayuan district; (c) Malichang district model; (d) Main cross-section in Malichang district; (e) Limei mineralized zone in Huayuan district; (f) Tudiping mineralized zone in Malichang district.

suitable. The implicit method has the strong capability of dynamic updatability, so it can be used to gradually model 3D processes using knowledge obtained in a sparse data field. In Part 2, we focused on volumetric calculations and demonstrated the value of 3D modelling at district and ore deposit scales for the prospectivity mapping of a stratabound mineral deposit. We constructed several models in the Huayuan-Malichang district, as shown in Fig. 16.

6. Summary and future work

In this contribution we have presented a resource estimation analogical method based on the mineral system modelling prospectivity approach. Based on the mineral system approach, we presented the assumption that the mean resources per unit (e.g., m^3) in a favourable area (defined as a trap in a mineral system) are consistent with the known ore-bearing zones (or fluid sinks) in the same mineral system. The formulas of undiscovered mineral resources were then transformed based on an analogy between the resources in favourable areas and the estimated reserves in ore-bearing zones with different levels of similarity. Furthermore, three variables were defined, i.e., the ore-bearing ratio, Similarity Index and volumes of the trap and ore-bearing zones. The ore-bearing ratio represents the mean resources per unit in representative deposits; the Similarity Index (or coefficient) is the quantification of how similar the association of favourable features in a trap is to the association of favourable features at representative ore deposits in the same mineral system. Then, a case study was conducted on multiple scales, i.e., the regional scale, district scale and ore deposit scale, based on the use of 2D GIS layers and 3D models (in Part 2) to verify the presence of stratabound ore deposits.

Herein, we discussed: (i) conceptual geological models, such as mineral systems and the descriptive mineral deposit model; (ii) digitalized favourable features are collected at the typical deposits in the study area; (iii) GIS-based prospectivity mapping was conducted in 2D from the regional scale (1:200,000) to the district scale (1:50,000); (iv) the volumes of favourable areas and ore-bearing zones are inferred at different scales; (v) similarities are calculated using Eqs. 10 or 11, and ore-bearing ratios are calculated using Eq. (5); and (vi) the undiscovered mineral resources inside traps are assessed using Eqs. (6) and (7).

This study employed the mineral system approach to analyse a theoretical “resource reservoir”, i.e., a permissive boundary, based on GIS-based 2D prospectivity modelling, such that the trap at the MVT Pb-Zn at Huayuan district was delineated. First, at the regional scale, we used the 1:200,000 datasets in Table 6 to delineate a favourable area within a GIS-based environment. Second, we refined the zones based on 1:50,000-scale datasets by combining the algal reef facies, Qingxudong Formation, and the “rough” boundary obtained from the regional scale (Table 6). Third, a method of analogy was then used to estimate the MVT Pb-Zn mineral resources in the Huayuan district: (i) the Similarity Index was calculated based on the association of favourable features in the district using the posterior probability of the BoostWofEs method or the Jarcard Index to compare the descriptive mineral deposit model in each unit cell; (ii) the arithmetic mean method was employed to determine the ore-bearing ratio; (iii) the volume was calculated using regular geometric models with empirical values obtained from representative cross-sections, such as Fig. 11, at both district and ore deposit scales; and (iv) the estimated resources were 63,531 t Pb and 3,667,509 t Zn when the WofE method was used and 79,231 t Pb and 4,573,836 t Zn when the Jarcard Index was used.

The main advantages of the analogical method include: (i) avoiding disputes in geological processes and ages because the method employs the mineral system approach to guarantee that the representative deposits are consistent with favourable areas; (ii) to directly use the results of the mineral system modelling prospectivity approach for the estimates of resources; (iii) to present the Similarity Index and available calculations such as the posterior probability or Jarcard Index to quantify subtle distinctions between representative deposits and permissive boundaries; and (iv) to easily extend the method of volume calculation using new technology, such as 3D modelling. However, this method still has some flaws, including: (i) it is difficult to be use in green-field scenarios because the method requires representative deposits; (ii) the formula of the ore-bearing ratio is linear, however, it is deliberate according to other methods, such as the 3-part method and Zipf’s law; and (iii) although its comparison to methodologies such as the 3-part method and Zipf’s law worked universally, the analogy method is only suitable for the mineral system prospectivity approach. Future work should further discuss and improve upon these points.

In addition, we will demonstrate a 3D modelling value of the undiscovered MVT Pb-Zn resources at Huayuan-Malichang district in Part II, as shown in Fig. 16, which adequately verifies the extendibility and compatibility of applying new technology to the assessment of mineral resources. Three-dimensional geometric models of the Qingxudong Formation, tectonic structures, and the Limei and Tudiping deposits are constructed now. This is followed by the interpretation of 3D geological models, the delineation of targets for mineralisation at depth, and, finally, the calculations of undiscovered mineral resources.

Acknowledgments

This research is financially supported by the National Natural Science Foundation of China (Project 41672330; NNSFC, http://www.nsfc.gov.cn/), Project No. 2017YFC0601501 from the National Key Research and Development Program of China, National Mineral Resources Assessment Initiative in China(1212011120140). We thank senior research fellow Leon Bagas for his encouragement and help during this study. We acknowledge the use of MRAS package for the modelling for GIS-based 2D prospectivity mapping at regional- and district- scales. We also appreciate the valuable comments of anonymous reviewers and editors.

Reference

Agterberg, F.P., 1993. Weights of evidence modeling and weighted logistic regression for mineral potential mapping. In: Davis, J.C., Herzfeld, U.C. (Eds.), Computers in Geology, 25 Years of Progress. Oxford University Press, Oxford, pp. 13–32.

Bliss, J.D., and Menzie, W.D., 1993. Spatial mineral deposit models and the prediction of undiscovered mineral deposits. In: Kirkham, R.V., Sinclair, W.D., Thorpe, R.I., Duke, J.M., eds. Mineral deposit modelling. Geological Association of Canada Special Paper 40, 693–706.

Bonham-Carter, G.F., Agterberg, F.P., 1989. Weights of evidence modelling: a new approach to mapping mineral potential. Geol. Sur. Can. 89, 171–183.

Bonham-Carter, G.F., 1994. Geographic Information systems for Geoscientist: Modeling with GIS. Oxford Elsevier pp. 398.

Boyer, C.M., Bai, Q.Z., 1998. Methodology of coalbed methane resource assessment. Int. J. Coal Geol. 35, 349–368.

Boulesteix, A.L., 2004. PLS dimension reduction for classification with microarray data. Stat Appl Genet Mol Biol 3 (1), 1–30.

Brown, W.M., Gedeon, T.D., Groves, D.I., Barnes, R.G., 2000. Artificial neural networks: a new method for mineral prospectivity mapping. Aust. J. Earth Sci. 47 (4), 757–770.

Carranza, E.J.M., Woldai, T., Chikambwe, M., 2005. Application of Data-Driven Evidential Belief Functions to Prospectivity Mapping for Aquamarine-Bearing Pegmatites, Lundazi District, Zambia. Nat. Resour. Res. 14 (1), 47–63.

Carranza, E.J.M., Hale, M., Faassen, C., 2008. Selection of coherent deposit-type locations and their application in data-driven mineral prospectivity mapping. Ore Geol. Rev. 33 (3), 536–558.

Carranza, E.J.M., Owusu, E.A., Hale, M., 2009. Mapping of prospectivity and estimation of number of undiscovered prospects for lode gold, southwestern Ashanti Belt, Ghana. Mineral. Depos. 44 (8), 915–938.

Chen, M., Sun, J., Fu, Y., Bao, Z., Bao, J., 2008. Geology and Geochemistry of Lead-Zinc Ore Zone and Prospecting Potential in Longshan County, Western Hunan. Resour. Environ. Eng. 22 (02), 151–158.

Cheng, Q.M., Agterberg, F.P., Bonham-Carter, G.F., 1996. Fractal pattern Integration for Mineral Potential Estimation. Nat. Resour. Res. 5, 117–130.

Cheng, Q.M., Agterberg, F.P., 1999. Fuzzy weights of evidence method and its application in mineral potential mapping. Nat. Resour. Res. 8, 27–35.

Cheng, Q.M., 2007. Mapping singularities with steam sediment geochemical data for prediction of undiscovered mineral deposits in Gejiu, Yunnan Province, China. Ore Geol. Rev. 32, 314–324.

Cheng, Q.M., 2015. BoostWofE: a new sequential weights of evidence model reducing the effect of conditional dependency. Math. Geosci. 47, 591–621.

Cheng, M., Hu, M., Bao, Z., Bao, J., 2011. Discussion on the Geological Features and Genesis of the Limei Pb-Zn ore Concentration Belt in North-western Hunan Province. Geol. Exp. 47 (2), 251–260.

China Geological Survey, 2013. Report of China national mineral resource potential estimate projects. China Geological Survey, Beijing, pp. 604–697.

Cong, Y., Dong, Q.J., Bagas, L., Xiao, K.Y., Wang, K., 2017;al., in press. Integrated GIS-based modelling for the quantitative prediction of magmatic Ti-V-Fe deposits: a case study in the Panzhihua-Xichang area of southwest China. Ore Geol. Rev in Press.

Cox, D.P., Singer, D.A., 1986. Mineral Deposit Models. U.S. Geological Survey Bulletin. United States Government Printing Office, Washington.

Cui, N., Sun, L., Bagas, L., Xiao, K.Y., Xia, J.S., 2017;al., in press. Geological

characteristics and analysis of known and undiscovered graphite resources of China. Ore Geol. Rev in Press.
Drew, L.J., 1997. Undiscovered petroleum and mineral resources, assessment and controversy: Plenum Press, New York, pp. 210
Feng, Z.Z., 1986. Early ordovician lithofacies and paleogeography in East North-China platform. Acta Sedimentol. Sin. 4 (4), 28–40.
Feng, Z.Z., Yang, Y.Q., Bao, Z.D., 1999. Lithofacies palaeogeography of the carboniferous in south China. J. Palaeogeogr. 1 (1), 75–86.
Feng, Z.Z., 2004. Single factor analysis and multifactor comprehensive mapping method – reconstruction of quantitative lithofacies palaeogeography. J. Palaeogeogr. 6 (1), 3–19.
Fu, S., 2011. Discussion on formation rules of high-grade Pb-Zn ore in Western Hunan. Nonferrous Metal. Min. Sect. 63 (6), 27–35.
González-Álvarez, I., Porwal, A., Beresford, S.W., McCuaig, T.C., Maier, W.D., 2010. Hydrothermal Ni prospectivity analysis of Tasmania, Australia. Ore Geol. Rev. 38 (3), 168–183.
Guj, P., Fallon, M., McCuaig, T.C., Fagan, R., 2011. A time-series audit of Zipf's Law as a measure of terrane endowment and maturity in mineral exploration. Econ. Geol. 106, 241–259.
Hagemann, S.G., Lisitsin, V.A., Huston, D.L., 2016. Mineral System analysis: Quo vadis. Ore Geol. Rev. 76, 504–522.
Hronsky, J.M.A., Groves, D.I., 2008. Science of targeting: definition, strategies, targeting and performance measurement. Aust. J. Earth Sci. 55, 3–12.
Huang, G.F., Jia, B.H., Sun, H.Q., Luo, X.Y., Tang, F.P., Chen, J., Su, Z.W., Tan, Y.H., Deng, Y.L., Yin, J.S., Yin, R.X., Yi, B.L., Li, S.M., Li, D.J., Ye, Y.Y., An, J.H., Zhou, G.X., Chen, B.H., He, C.P., Shi, J.J., Xiao, D.G., Li, Z.H., Zi, B.Z., Huang, F.Q., Zeng, F., Peng, C., Yao, Y.J., Duan, L., 2011. China's national mineral resource assessment achievement report: mineral potential mapping in Hunan Province. Hunan Inst. Geol. Sur. 253–310.
Jaccard, P., 1901. Distribution de la flore alpine dans le Bass in des Dranses et dams-quelque region vasines. Bull. Soc. Vaud. Sci. Nat. 37, 241–272.
Joly, A., Porwal, A., McCuaig, T.C., 2012. Exploration targeting for orogenic gold deposits in the Granites-Tanami Orogen: mineral system analysis, targeting model and prospectivity analysis. Ore Geol. Rev. 48, 349–383.
Joly, A., Porwal, A., McCuaig, T.C., Chudasama, B., Dentith, M.C., Aitken, A.R.A., 2015. Mineral systems approach applied to GIS-based 2D-prospectivity modelling of geological regions: insights from Western Australia. Ore Geol. Rev. 71, 673–702.
Kingston, G.A., David, M., Meyer, R.F., Oeenshine, A.T., Slamet, S., Schanz, J.J., 1978. Workshop on Volumetric Estimation. Math. Geol. 10, 495–499.
Knox-Robinson, C.M., 2000. Vectorial fuzzy logic: a novel technique for enhanced mineral prospectivity mapping, with reference to the orogenic gold mineralisation potential of the Kalgoorlie Terrane, Western Australia. Aust. J. Earth Sci. 47 (5), 929–941.
Li, S.M., 2016. Research on Metallogenic Regularities and prognosis of Lead-zinc Deposits in Northwestern Hunan. PhD Thesis. China University of Geoscience, Beijing.
Liu, Y.P., Xia, Y., Wang, J.M., 2010. Metallogenic characteristics and metallogenic factors of bauxite deposits in Northern Guizhou province. Bull. Miner. Petrol. Geochem. 29 (4), 422–425.
Lorber, A., Wangen, L.E., Kowalski, B.R., 1987. A theoretical foundation for the PLS algorithm. J. Chemom. 1 (1), 19–31.
McCuaig, T.C., Beresford, S., Hronsky, J.M.A., 2010. Translating the mineral systems approach into an effective exploration targeting system. Ore Geol. Rev. 38 (3), 128–138.
McCuaig, T.C., Hronsky, J.M.A., 2014. The Mineral System Concept: the key to exploration targeting. Soc. Econ. Geol. Spec. Issue 18, 153–175.
Merriam, D.F., Drew, L.J., Schuenemeyer, J.H., 2004. Zipf's Law: a Viable Geological Paradigm? Nat. Resour. Res. 13 (4), 265–270.
Meyer, R.F., 1978. The volumetric method for petroleum resource estimation. Math. Geol. 10, 501–518.
Perrouty, S., Lindsay, M.D., Jessell, M.W., Aillères, L., Martin, R., Bourassa, Y., 2014. 3D modeling of the Ashanti Belt, southwest Ghana: Evidence for a litho-stratigraphic control on gold occurrences within the Birimian Sefwi Group. Ore Geol. Rev. 63, 252–264.
Porwal, A., Carranza, E.J.M., Hale, M., 2003a. Artificial neural networks for mineral potential mapping. Nat. Resour. Res. 12 (3), 1–15.
Porwal, A., Carranza, E.J.M., Hale, M., 2003b. Extended Weights-of-evidence modeling for predictive mapping of base-metal deposit potential in Aravalli Province, Western India. Expl. Min. Geol. 10 (4), 155–163.
Porwal, A., Carranza, E.J.M., Hale, M., 2003c. Knowledge-driven and data-driven fuzzy models for mineral potential mapping. Nat. Resour. Res. 12 (1), 1–25.
Porwal, A., Carranza, E.J.M., Hale, M., 2004. A hybrid neuro-fuzzy model for mineral potential mapping. Math. Geol. 36 (7), 803–826.
Porwal, A., Carranza, E.J.M., Hale, M., 2006a. A hybrid fuzzy weights-of-evidence model for mineral potential mapping. Nat. Resour. Res. 15, 1–14.
Porwal, A., Carranza, E.J.M., Hale, M., 2006b. Bayesian network classifiers for mineral potential mapping. Comput. Geosci. 32 (1), 1–16.
Porwal, A., González-Álvarez, I., Markwitz, V., McCuaig, T.C., Mamuse, A., 2010. Weights-of-evidence and logistic regression modeling of magmatic nickel sulfide prospectivity in the Yilgarn Craton. West. Australia 38 (3), 184–196.
Porwal, A., Carranza, E.J.M. 2015. Introduction to the Special Issue: GIS-based mineral potential modelling and geological data analyses for mineral exploration, Ore Geol. Rev. 71, pp. 477–483.
Singer, D.A., 1993. Basic concepts in three-part quantitative assessments of undiscovered mineral resources. Non-renew. Resour. 2, 69–81.
Singer, D.A., Kouda, R., 1996. Application of Feedforward Neural Network in the Search for Kuroko Deposits in the Hokuroku District. Japan Mathemat. Geol. 28 (8), 1017–1023.
Singer, D.A., Kouda, R., 2001. Some simple guides to finding useful information in exploration geochemical data. Nat. Resour. Res. 10 (2), 137–147.
Singer, D.A., 2006. Typing mineral deposits using their associated rocks, grades and tonnages using a probabilistic neural network. Math. Geol. 38 (4), 465–474.
Singer, D.A., 2008. Mineral deposit densities for estimating mineral resources. Math. Geol. 40, 33–46.
Singer, D.A., Menzie, W.D., 2010. Quantitative mineral resource assessments—An integrated approach: Oxford University Press, New York, pp. 219.
Tang, J.X., Wang, D.H., Wang, X., Zhong, K., Ying, L., Zheng, W., Li, F., Guo, N., Qin, Z., Yao, X., Li, L., Wang, Y., Tang, X., 2010. Geological features and metallogentic model of the Jiama copper-polymetallic deposit in Tibet. Acta Geosci. Sin. 31, 495–506 (in Chinese).
Tripathi, V.S., 1979. Factor analysis in geochemical exploration. J. Geochem. Explor. 11, 263–275.
Voroshilov, V.G., 2009. Anomalous structures of geochemical fields of hydrothermal gold deposits: Formation mechanism, methods of geometrization, typical models, and forecasting of ore mineralisation. Geol. Ore Depos. 51 (1), 1–16.
Wang, H.W., 1999. Partial Least Squares Regression and Its Application. National Defence Industry Press, Beijing, China.
Wang, G.W., Li, R., Carranza, E.J., Zhang, S., Yan, C.H., Zhu, Y., Qu, J., Hong, D., Song, Y., Han, J., Ma, Z., Zhang, H., Yang, F., 2015. 3D geological modeling for prediction of subsurface Mo targets in the Luanchuan district, China. Ore Geol. Rev. 71, 592–610.
Wang, K., Li, N., Bagas, L., Li, S.M., Song, X.L., Cong, Y., 2017;al., in press. GIS-based prospectivity-mapping based on geochemical multivariate analysis technology: a case study of MVT Pb–Zn deposits in the Huanyuan-Fenghuang district, Northwestern Hunan Province, China. Ore Geol. Rev. 91, 1130–1146.
Wang, S.C., Fan, J.Z., Yang, H., 1990. Mineral Resources Evolution. Jilin Science and Technology Publishing House, Changchun.
Wold, S., Ruhe, H., Wold, H., 1984. The collinearity problem in linear regression. The partial least squares(PLS) approach to generalized inerses. SIAM J. Scient. Stat. Comput. 5 (03), 735–743.
Wyborn, L.A.I., Heinrich, C.A., Jaques, A.L., 1994. Australian Proterozoic mineral systems: essential ingredients and mappable criteria. In: Hallenstein, P.C. (Ed.), Australian Mining Looks North — the challenges and choices. Australian Institute of Mining and Metallurgy Publication Series 5.
Xiao, K.X., Xing, S.W., Bagas, L., Sun, L., Li, N., Yin, J.N., Cui, N., Cong, Y., Li, J., Chen, Y.C., Ye, T.Z., 2017;al., in press. The China National Mineral Assessment Initiative. Ore Geol. Rev in Press.
Xue, C.J., 2015. Research on Metallogenic Regularities and prognosis of Lead-zinc Deposits in Northwestern Hunan. PhD' thesis. China University of Geoscience, Xian.
Yang, S., 2003. Analysis on the prospecting foreground for Pb-Zn deposits in West Hunan. Hunan Geol. 22 (02), 107–111.
Yang, S., Lao, K., 2007. Geological characteristics and ore indicators of lead-zinc deposits in northwestern Hunan, China. Geol. Bull. China 26 (7), 899–908.
Yuan, 2013. Perspectivity reserves at Huyuan-Fenghuang district, Hunan province, China. Mech. Eng. 6, 1–11.
Zhang, X.Y., Peng, Y.Y., Xiong, Y.W., Cao, S.H., Zou, G.J., Li, C., Zhou, G.X., He, C.P., Li, H.J., 2013. Report of Regional Geological Survey (1:50,000) in the Huayuan District, Malichang District, Heku District, Duoxi District. People's Republic of China. Hunan Institute of Geological Survey.
Zhang, S.H., Xiao, K.Y., Zhu, Y.S., Cui, N., 2017;al., in press. A prediction model for important mineral resources in China. Ore Geol. Rev in Press.
Zhao, P.D., Chen, J.P., Chen, J.G., 2001. Introduction to "Three step" Digital Mineral Prospecting and assessment. Procee. Int. Symp. 1–5.
Zhao, P.D., 2002. "Three step" quantitative forecasting and assessment of resource-theory of digital exploration and discussion on practice. Earth Sci. 27, 482–489 (in Chinese with English Abstract).
Zhao, P.D., Chen, J.P., Zhang, S.T., 2003. The new development of "three components" quantitative mineral prediction. Earth Sci. Front. 2, 455–463 (in Chinese with English Abstract).
Zhong, J.S., Mao, C.M., 2007a. Discuss on the characteristics and metallogenic mechanism of MVT lead-zinc deposit in western Hunan. Land Resour. Herald 4 (2), 52–56.
Zhong, J., Mao, C., 2007b. Features and metallogenic mechanism of MVT Pb-Zn deposits in North western Hunan. Land Resour. Herald 4 (06), 52–56.
Zhu, Y.S., 1997. Prospectivity Mapping Methods. Geological Publish House, Beijing.